

# **THE VALIDATION OF RESOLVE HELICOPTER EM DATA: MINERALOGICAL AND PETROPHYSICAL RESULTS FROM FIELD INVESTIGATIONS FOR THE TINTINARA EAST SURVEY AREA, IN THE SOUTH EAST OF SOUTH AUSTRALIA**



*K.P Tan, T. Munday and F. Leaney*

**CRC LEME OPEN FILE REPORT 174**

**September 2004**



# **THE VALIDATION OF RESOLVE HELICOPTER EM DATA: MINERALOGICAL AND PETROPHYSICAL RESULTS FROM FIELD INVESTIGATIONS FOR THE TINTINARA EAST SURVEY AREA, IN THE SOUTH EAST OF SOUTH AUSTRALIA**

*K.P Tan, T. Munday and F. Leaney*

**CRC LEME OPEN FILE REPORT 174**

September 2004

*Report prepared for the South Australia Salinity Mapping and  
Management Support Project.*

*This project is jointly funded by the South Australian and Commonwealth  
Governments under the National Action Plan for Salinity and Water Quality.*

© CRC LEME 2004

---

CRC LEME is an unincorporated joint venture between CSIRO-Exploration & Mining, and Land and Water, The Australian National University, Curtin University of Technology, University of Adelaide, Geoscience Australia, Primary Industries and Resources SA, NSW Department of Mineral Resources and Minerals Council of Australia.

*Headquarters:* CRC LEME c/o CSIRO Exploration and Mining, PO Box 1130, Bentley WA 6102, Australia

**Copies of this Publication can be obtained from :**

The publications Officer, CRCLEME, c/- CSIRO Exploration and Mining, PO Box 1130, Bentley WA 6120, Australia. Information on other publications in this series may be obtained from the above, or from <http://crcleme.org.au>

**Cataloguing-in-Publication:**

Name: Tan, K.P, Munday T.J. and Leaney, F.W.J., Title: The validation of RESOLVE Helicopter EM data: mineralogical and petrophysical results from field investigations for the Tintinara East Survey area in the South East of South Australia  
ISBN 1 921039 12 4

1. East Tintinara, South Australia    2. AEM    3. Petrophysics

I. Name II. Title

CRCLEME Open File Report 174

ISSN 1329-4768

**Address and Affiliation of Authors**

**KP Tan**

Cooperative Research Centre for Landscape  
Environments and Mineral Exploration  
c/-Geoscience Australia  
GPO Box 378,  
Canberra, ACT 2601  
Australia

**Tim Munday**

Cooperative Research Centre for Landscape  
Environments and Mineral Exploration  
c/- CSIRO Exploration and Mining  
26 Dick Perry Avenue,  
Technology Park,  
Kensington, Western Australia 6151  
Australia.

**Fred Leaney**

CSIRO Land and Water  
PMB 2  
Glen Osmond  
South Australia 5064  
Australia

## Table of Contents

|        | <b>Page</b>   |
|--------|---|
| I      | Table of Contents..... 1  |
| II     | List of Figures..... 2  |
| III    | List of Tables..... 4   |
| IV     | Abstract..... 5   |
| 1.     | Introduction..... 7   |
| 1.1    | Background..... 7   |
| 1.2    | Study Area..... 8   |
| 1.3    | Hydrogeology..... 10  |
| 2.     | Objectives..... 11  |
| 3.     | Geophysical Data Acquisition, Modelling and Inversion..... 12                 |
| 3.1    | Forward Modelling..... 12   |
| 3.2    | HEM System and Survey Parameters..... 12                                      |
| 3.3    | Inversion..... 12   |
| 4.     | Ground Validation and Targeted Drilling..... 16                               |
| 5.     | Results..... 17   |
| 5.1    | Borehole TIN1LC..... 17   |
| 5.2    | Borehole TIN3HC..... 17   |
| 5.3    | Borehole TIN4HC..... 18   |
| 5.4    | Borehole TIN5LC..... 18   |
| 5.5    | Borehole TIN6HC..... 19   |
| 5.6    | Petrophysical Attributes..... 25  |
| 5.6.1  | Water Content..... 25   |
| 5.6.2  | Chloride Concentrations..... 25   |
| 5.6.3  | Grain Size Distribution, Clay Abundance and Mineralogy... 26                  |
| 5.6.4  | Electrical Conductivity..... 27   |
| 6.     | Discussion..... 29  |
| 6.1    | Causal Relations amongst the Petrophysical Attributes..... 29                 |
| 6.2    | Validation and interpretation of CDI image..... 32                            |
| 6.3    | Validation of constrained inversion product – Clay Thickness<br>Image..... 34 |
| 7.     | Conclusion..... 39  |
| 8.     | References..... 40  |
| 9.     | Acknowledgements..... 42  |
| 10     | Appendices..... 43  |
| 10.1   | Appendix 1 – Methods..... 43  |
| 10.1.1 | Bores..... 43   |
| 10.1.2 | Down-hole Electrical Conductivity Log..... 43                                 |
| 10.1.3 | Down-hole Gamma Log..... 43   |
| 10.1.4 | Grain Size Distribution..... 43   |
| 10.1.5 | Mineral Composition..... 45   |
| 10.2   | Appendix 2 – Results..... 46  |

| <b>List of Figures</b> |   | <b>Page</b> |
|------------------------|---|-------------|
| Figure 1a.             | Distribution of salt in the soil and groundwater under natural vegetation.....  | 7           |
| Figure 1b              | Leaching of salt due to clearing/irrigation and higher recharge.....  | 7           |
| Figure 1c.             | Movement of salt to the irrigation bore and mixing with fresher groundwater. ....   | 7           |
| Figure 2.              | Landsat TM pseudo-coloured image showing the AEM survey areas, <i>i.e.</i> Tintinara East, Tintinara West and Riverland.....                              | 9           |
| Figure 3.              | Block diagram of the Tintinara-Coonalpyn Prescribed Wells Area....  | 10          |
| Figure 4.              | RESOLVE <sup>®</sup> HEM interval conductivity for 8-10m below the surface, derived from a CDI transformation of those data.....                          | 13          |
| Figure 5.              | Block model of RESOLVE Interval conductivity for 8-10m draped on topography, with a geological interpretation of the observed conductivity structure..... | 13          |
| Figure 6.              | 1D Layered Earth conductivity depth section from the constrained inversion of one flight line.....  | 14          |
| Figure 7.              | Map of the clay thickness derived from the constrained 1D LEI of RESOLVE HEM data.....  | 15          |
| Figure 8.              | Borehole TIN1LC.....  | 20          |
| Figure 9.              | Borehole TIN3HC.....  | 21          |
| Figure 10.             | Borehole TIN4HC.....  | 22          |
| Figure11.              | Borehole TIN5LC.....  | 23          |
| Figure 12.             | Borehole TIN6HC.....  | 24          |
| Figure 13a.            | Frequency histograms of water content distribution .....  | 25          |
| Figure 13b.            | Box plots of water contents in each lithologic unit.....  | 25          |
| Figure 14a.            | Frequency histograms of chloride concentrations.....  | 26          |
| Figure 14b.            | Box plots of chloride concentrations in each lithologic unit.....   | 26          |
| Figure 15a.            | Frequency histograms of clay abundance.....   | 27          |
| Figure 15b.            | Box plots of clay abundance in each lithologic unit.....  | 27          |
| Figure 15c.            | Ternary plot showing the sedimentary textures.....  | 27          |
| Figure 16a.            | Frequency histograms of apparent electrical conductivity.....   | 28          |
| Figure 16b.            | Box plots of apparent electrical conductivity in each lithologic unit... ..   | 28          |
| Figure 17a.            | Positive correlation between water content and clay abundance.....  | 31          |
| Figure 17b.            | Positive correlation between electrical conductivity and water content.....   | 31          |
| Figure 17c.            | Positive correlation between electrical conductivity and salt load.....   | 31          |
| Figure 17d.            | Positive correlation between electrical conductivity and clay Abundance.....  | 31          |
| Figure 17e.            | Improved correlation of electrical conductivity and clay abundance by Removing outlier groups.....  | 31          |
| Figure 18a.            | Closed up view of the electrical conductivity patterns in the vicinity of bore TIN1LC.....  | 33          |
| Figure 18b.            | Closed up view of the electrical conductivity patterns in the vicinity of bore TIN3HC.....  | 33          |
| Figure 18c.            | Closed up view of the electrical conductivity patterns in the vicinity of bore TIN4HC.....  | 33          |
| Figure 18d.            | Closed up view of the electrical conductivity patterns in the vicinity of bores TIN5LC and TIN6HC.....  | 33          |
| Figure 19a.            | Predicted clay thickness (5 m) from the Clay Thickness Image.....   | 35          |
| Figure 19b.            | Predicted clay thickness (10 m) from the Clay Thickness Image.....  | 35          |
| Figure 19c.            | Predicted clay thickness (15 m) from the Clay Thickness Image.....  | 36          |

|             |   |    |
|-------------|---|----|
| Figure 19d. | Predicted clay thickness (20 m) from the Clay Thickness Image.....  | 36 |
| Figure 20.  | Schematic diagram showing the sedimentary relationships and the distribution of fine-textured back barrier sediments..... | 37 |
| Figure 21.  | CDI at 8-10 m depth showing the area occupy by the Ngarkat conservation park.....   | 38 |
| Figure 22.  | Schematic diagram shows the main components of a laser diffractometer (Malvern Instruments).....                          | 44 |

## List of Tables

|   | <b>Page</b> |
|---|-------------|
| Table 1. Initial assumptions about the conductivity structure in the Tintinara area.....          | 14          |
| Table 2. Table shows the boreholes coordinates and drill depths.....                              | 16          |
| Table 3. Average electrical conductivity at 6 to 8 m depths of the five validation boreholes..... | 32          |
| Table 4. Thickness of conductive sediments of the Pliocene lagoonal facies.....                   | 34          |
| Table 5. Particle size in SI units ( $\mu\text{m}$ ).....   | 45          |
| Table 6. Grain size distribution of sediments and the respective lithologic units.....            | 46          |
| Table 7. Mineral composition of sediments and the respective lithologic units.....                | 48          |

## ABSTRACT

As part of the South Australian Salinity Mapping and Management Support Project (SA-SMMSP), helicopter airborne electromagnetic (HEM) data of the Tintinara East, have been acquired to map subtle conductivity variations in near surface materials (~1-10 m) at a high spatial resolution as an aid to managing the existing groundwater resource. In the absence of much surface water, the groundwater resources at Tintinara represent an important asset. The lifetime of this resource is not limited by the volume of abstraction, but by increasing salinity due to irrigation practices. Salt that has accumulated in the soil and sediments is being leached by increased recharge, exacerbated by the recent increase in irrigation. The presence or absence of a near surface clay unit is important. In the presence of a thick clay unit, the impacts of irrigation on the aquifer will be over a period of hundreds of years. A management strategy being developed for the region involves steering new irrigation development to those areas of thicker, near surface, clay layers, targeting water use efficiency. In areas where clay is absent, relocating irrigation-based enterprises to more appropriate sites may be necessary, in order to significantly prolong the lifetime of the groundwater resource.

This study had four objectives:

1. To define the principal factors driving variations in observed electrical conductivity in the sediments of the Tintinara East study area.
2. To provide appropriate geo-electrical constraints for the conduct of a constrained inversion of the HEM data to better map the distribution of the shallow clay.
3. To ascertain whether the conductivity depth image (CDI's, e.g. 6 - 8 m) reflects the distribution of conductive clay materials, which, in the vicinity of the study area, are associated with the fine textured back-barrier sedimentary facies of the Pliocene Loxton-Parilla Sands.
4. To verify whether the constrained inversion product, *i.e.* the Clay Thickness Image was a good representation of true clay thickness.

Five boreholes were selected to target the various conductivity responses observed in the conductivity-depth intervals generated from the inversion of the HEM data. Both field and laboratory analyses were employed, including down-hole conductivity logs and measurement of water and chloride content, as well as a determination of grain size distribution in sampled materials. An examination of the drill cuttings in light of the regional geology suggests that four lithologic units are represented in the study area, including the Molineaux-Lowan Sands (Quaternary), Bridgewater Formation (Quaternary), Loxton-Parilla Sands (Pliocene) and time equivalent fine-textured lagoonal facies sediments.

From correlation of the inverted HEM data with borehole information, and statistical analyses carried out on the petrophysical attributes of the lithologic units, the following can be concluded.

1. In the Tintinara AEM survey area, the primary driving factor of electrical conductivity is salt load, which is a function of water content and its salinity. Electrical conductivity is correlated to clay abundance due to the positive causal relationship of the latter with water content, which denotes the degree of saturation of pore spaces in the sediments.

2. The 25<sup>th</sup> percentile of 240 mS/m of the fine-textured lagoonal facies sediments can be used as a threshold value in differentiating between conductive and resistive sediments. From line of regression, 240 mS/m will equate to approximately 24 vol. % clay. The sedimentary texture ternary diagram indicates that samples containing more than 24 vol. % clay comprise sandy mud and sandy clay. Since the sands (*i.e.* muddy sand and sand) are dominantly resistive with only a handful of wet and conductive saline sand units, it is possible to utilize electrical conductivity to map the conductive mud and clay.
3. The relationship between the geological units and their respective electrical conductivity suggest the adoption of a three layer model for constraining the inversion of HEM data. The layers comprises a resistive layer 1 (Molineaux-Lowan Sands), a conductive layer 2 (lagoonal facies) and a resistive layer 3 (Loxton-Parilla Sands).
4. Evidence from textural information and borehole conductivity logs, as obtained from the 5 selected boreholes which targeted specific conductivity signatures shown on the CDI (6-8 m depth slice) and the clay thickness product derived from the constrained inversion, confirms that the Helicopter EM system used at Tintinara was successful in mapping near surface clay-rich materials. The conductivity patterns suggest the presence of paired linear resistors comprising barrier sand, which is accompanied by conductive back-barrier fine-textured sediments.

## 1. INTRODUCTION

### 1.1 Background

In response to an increased interest in developing irrigated agriculture (e.g. lucerne, vegetables and olives) in the SE region of South Australia, the SA Government Department of Water, Land and Biodiversity Conservation (DWLBC) has initiated a series of studies on the available groundwater resource as part of a broader management strategy for the area (Barnett, 2002). In the absence of much surface water, the groundwater resources represent an important asset, and this is of particular significance in the Tintinara-Coonalpyn Prescribed Wells Area (TCPWA). Here, the lifetime of the available groundwater resource is not limited by the volume of extraction, but rather to the detrimental effect on water quality of increasing salinity; a direct consequence of land clearing and increased recharge due to dryland agriculture.

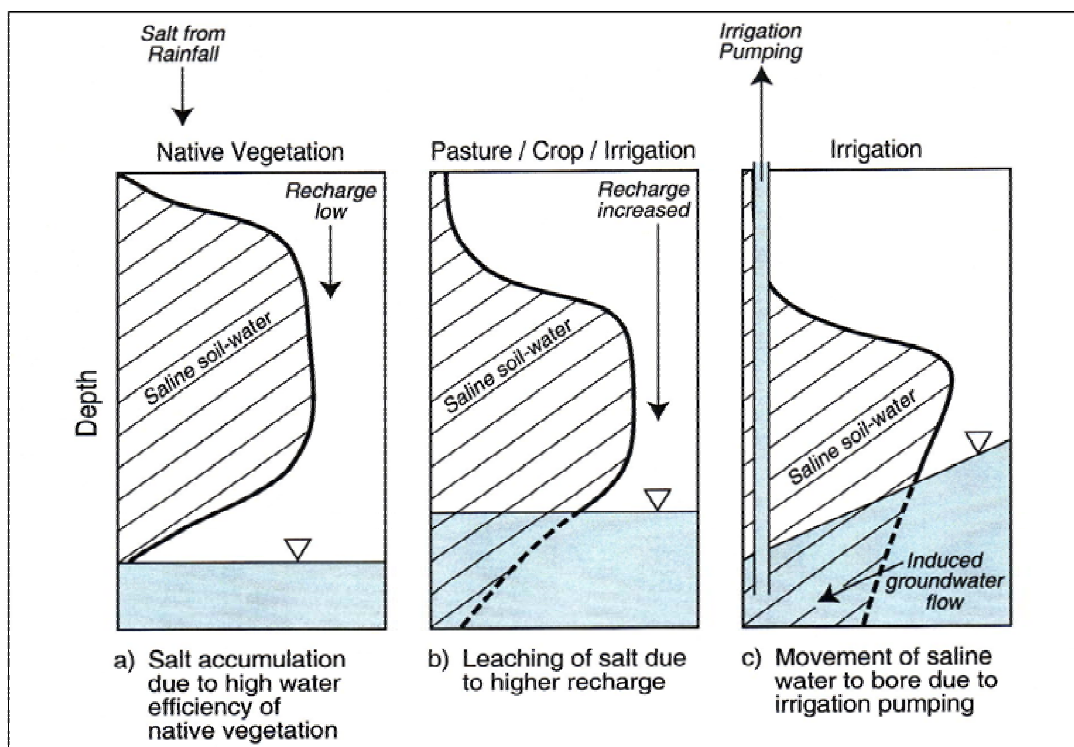


**Figure 1.** a) Distribution of salt in the soil and groundwater under natural vegetation, b) leaching of salt due to clearing/irrigation and higher recharge and c) Movement of salt to the irrigation bore and mixing with fresher groundwater. An increase in the salinity of irrigation water results (source Leaney et al. 1999)

The TCPWA, which covers an area of  $\sim 3423\text{km}^2$ , can be divided into two areas, the low-lying coastal plain to the west and the highlands of the Mallee to the north and east, each characterized by different aquifer systems and, on the basis of different hydrogeological processes, each requiring different management approaches. In the Mallee highlands, to the north and east of Tintinara, rising trends in groundwater salinity have been noted. These increases follow land clearing and the lack of recycling of irrigation water. Salt that occurred in rainfall was concentrated by the native Mallee vegetation and stored in the root zone. It is now being flushed down to the deep watertable (Leaney et al., 1999). It has been suggested that drainage from

irrigated areas will accelerate the process of salinisation (Leaney, 2000), depending on the efficiency of the irrigation. The mechanisms involved are summarized in Figure 1. For some areas, the groundwater may be unusable for irrigation within the vicinity of the development within ten to twenty years. However, these studies have indicated that very efficient irrigation, especially on heavier (clay-rich) soils, will barely increase drainage above non-irrigated recharge rates, if at all. Therefore the presence or absence of near surface clays is important. In the presence of a thick clay unit, the impacts of irrigation on the aquifer will be over a longer time period (~ 50-100 years). Presently, a management strategy developed for the region involves steering new irrigation development to those areas of thicker, near surface, clay layers, targeting water use efficiency. In areas where clay is absent, relocating irrigation-based enterprises to more appropriate sites may be necessary, with intent to significantly prolong the lifetime of the groundwater resource.

Our current knowledge of the distribution and thickness of the near surface clay units is derived from borehole data, which although relatively extensive, does not have adequate ancillary information on the texture and clay content of near surface materials appropriate for planning purposes. To help address this shortcoming, helicopter airborne electromagnetic (HEM) data were acquired over part of the TCPWA, under the auspices of the South Australian Salinity Mapping and Management Support Project (SA-SMMSP) ([www.saltcontrols.com/salt\\_mapping.htm](http://www.saltcontrols.com/salt_mapping.htm)). The intent of the geophysical survey was to map near-surface zones of relatively high conductivity associated with clay-rich materials quickly and economically. Of particular importance was the need to identify areas with significant thicknesses of clay. This product was to be used as a basis for modelling the spatial variability of recharge to the groundwater across the study area, along with the salt flux.

In the TCPWA, the SA-SMMSP considered the application of geophysics from an understanding of regional variations in landscape, hydrogeology, land use and the requirements of a particular community. The blanket acquisition of geophysical data was not entertained. At the outset, recognition was given to benefits of acquisition by particular systems at particular scales, given cognisance of the targets and the resource needs of the decision makers. In this regard, the SA-SMMSP represents a significant departure from previous studies seeking to apply airborne geophysics in land management. It also reflects the thinking promoted earlier on the relevance of geophysics in land management (George and Green, 2000). A critical part of the project planning process has been to ensure that those biophysical data generated (*i.e.* a map of clay thickness) can be used as an input into groundwater models that will have significant economic impact, be influential in developing land management plans, and where the recommendations of planning are likely to be adopted by landholders.

## 1.2 Study Area

This paper describes results obtained from the acquisition and inversion of RESOLVE<sup>®</sup> HEM data inversion of HEM data acquired over the Mallee Highlands Zone, east of the Tintinara township (Figure 2), one of two areas flown in the TCPWA. The Mallee Highlands consist of undulating plains that increase in height to the east, reaching an elevation of >100 mAHD. The contemporary land surface is dominated by east-west trending dunes referred to by Brown and Stephenson (1991) as the Molineaux-Lowan Sands. Soils in the area are generally sandy, although clay soils are more common in the inter-dune depressions (Leaney et al., 1999).

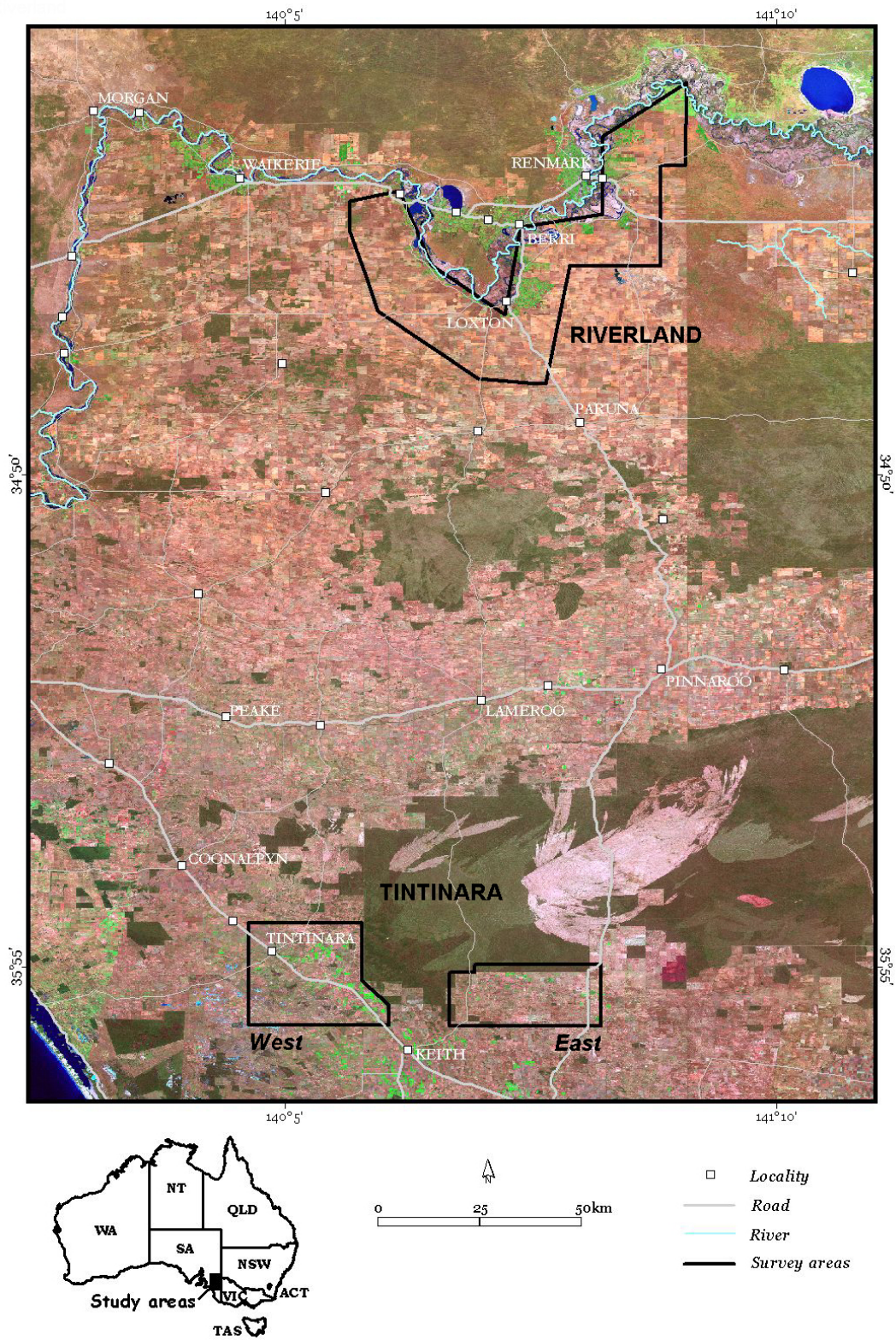


**Figure 2.** Landsat TM pseudo-coloured image showing the AEM survey areas, *i.e.* Tintinara East, Tintinara West and Riverland.

### 1.3 Hydrogeology

Surface water is absent from the Tintinara East study area, and therefore groundwater provides the main water resource in the region. Located on the southwest margin of the Murray Basin, groundwater flows through two major aquifer systems: a regionally unconfined limestone aquifer and an underlying confined aquifer with sand and bryozoal limestone (coral) layers. The two aquifers are separated by a low permeability aquitard usually made up of a dark-brown carbonaceous clay. The aquifers are hydraulically connected, but the degree of hydraulic connectivity is poorly understood. (Barnett 2002). The upper, unconfined limestone aquifer is the more extensively used of the two aquifers. However, poor groundwater quality in this aquifer in some areas has resulted in the development of the underlying confined aquifer as a water resource.

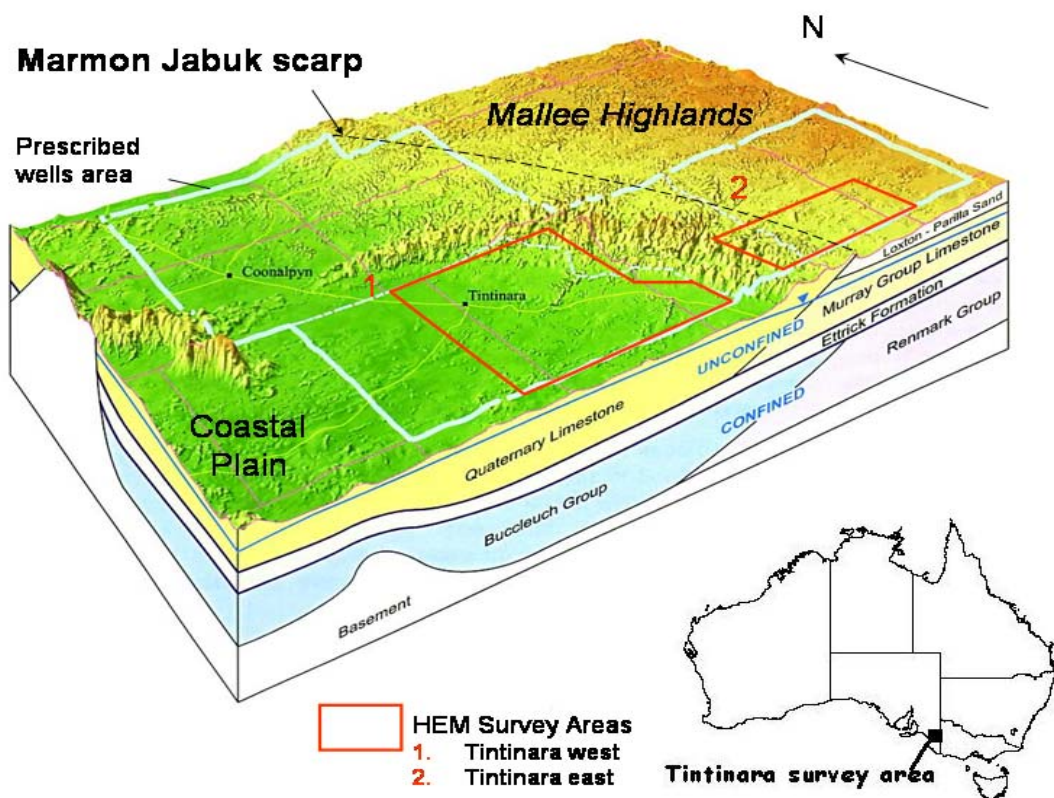


**Figure 3.** Block diagram of the Tintinara-Coonalpyn Prescribed Wells Area, showing the location of the HEM surveys areas in relation to the local geomorphology and hydrogeology (adapted from Barnett 2002).

The Tintinara East survey area straddles the Marmon-Jabuk scarp (Figure 3) and part of the flat low-lying coastal plain which formed from a regressive-transgressive cycle at the end of the Pliocene and early Pleistocene following uplift in the mid-late Pliocene. Erosion of the Murray Group Limestone and Pliocene Loxton-Parilla sands which underlie the higher Mallee landscape to the northeast, was followed by deposition of the carbonate-rich Bridgewater Formation which now makes up part of a regionally extensive unconfined limestone aquifer. The confined aquifer consists of quartz sands and bryozoal limestone layers, interbedded with dark-brown

carbonaceous clays. The limestone layers occur in the Buccleuch Formation, whose extent approximates that of the Coastal Plain. This unit merges laterally with the Renmark Group of the Murray Basin.

## **2. OBJECTIVES**

The primary objective of this study was to validate causes for the observed conductivity structure in the RESOLVE HEM data and provide the basis for their interpretation. The intent was to further validate these data as an effective technology for mapping near surface “clay” rich sedimentary units that would influence recharge rates to the groundwater.

The study had four objectives:

1. To define the principal factors driving variations in electrical conductivity in the sediments of the Tintinara East study area.
2. To provide appropriate geo-electrical constraints for the conduct of a constrained inversion of the HEM data to better map the distribution of the shallow clay.
3. To ascertain whether the conductivity depth interval images (CDI's, e.g. 6 - 8 m) reflect the distribution of conductive clay materials, which, in the study area, are associated with the fine textured back barrier sedimentary facies of the Pliocene Loxton-Parilla Sands.
4. To verify the constrained inversion product, particularly the Clay Thickness Image (CTI), for mapping the thickness of the clay, and identify the presence of any outliers.

### **3. GEOPHYSICAL DATA ACQUISITION, MODELLING AND INVERSION**

#### **3.1 Forward Modelling**

A scoping study conducted on ground and borehole data from the Mallee Highlands Zone indicated that the clay units were characterised by elevated electrical conductivities relative to overlying dune sands and underlying sandy sediments. A forward modelling exercise using this information concluded that high resolution (helicopter) airborne EM systems could map the presence, or absence, of these near-surface units provided they were thick, or conductive, enough. Results from a similar exercise conducted for another study area in South Australia (Munday *et al.*, 2003), concluded that the best results would be obtained from flying the RESOLVE<sup>®</sup> HEM system over the area.

#### **3.2 HEM System and Survey Parameters**

Data were successfully acquired for two survey areas around Tintinara with a line spacing of 300m. A total of the 1669 line kms were flown for the Tintinara East area with an east-west line orientation. Whilst the broader line spacing meant that we were less likely to resolve some of the variability associated with the near surface clay materials, the detail likely to be generated would still be much greater than that possible through drilling. The HEM system was particularly suited to the more hilly country east of Tintinara.

The RESOLVE<sup>®</sup> HEM system is a six frequency EM system mounted in a bird towed beneath a helicopter. The bird contains horizontal coplanar coils, and in the Tintinara survey measured an EM response at 385 Hz, 1518 Hz, 6135 Hz, 25380 Hz and 106140 Hz (Cowey *et al.*, 2003). It also has one coaxial coil pair which measured a response at 3323 Hz. The RESOLVE<sup>®</sup> is a fully digital EM system, offering improved signal:noise characteristics, real-time signal processing as well as internal calibration coils for automatic phase and gain calibration in the air. These characteristics result in higher accuracy and a reduced drift. The very high frequencies help resolve very near surface conductors as might be represented by the clay-rich near-surface materials found at Tintinara.

#### **3.3 Inversion**

Once acquired, these data were processed to apparent conductivities and thicknesses using a pseudo-layer half-space model (Fraser 1978). They were also inverted using the Conductivity Depth Imaging (CDI) method (Macnae *et al.* 1998). Figure 4 shows an interval conductivity slice for a depth interval of 8-10m derived from the CDI's generated by EMFlow software.

The image maps several zones of relatively high conductivity (~500 mS/m), orientated in a roughly NE-SW direction. These high conductivity zones are separated by more linear resistive zones. The conductivity structure, defined by these approximate methods, helped to determine the geological evolution of the area, and contributed to the definition of appropriate limits when we attempted to invert the data using a constrained 1D layered earth model. Specifically the CDI's resolved a beach strandplain structure associated with the Loxton-Parilla Sands which overlie the Murray Group Limestones (Figure 5) (Brown and Stephenson, 1991). The linear resistive structures mentioned above were ascribed to a coarser sand of the upper shoreface facies of the barrier complexes. The conductive zones were attributed to back-barrier lagoonal clays between individual barrier sands.

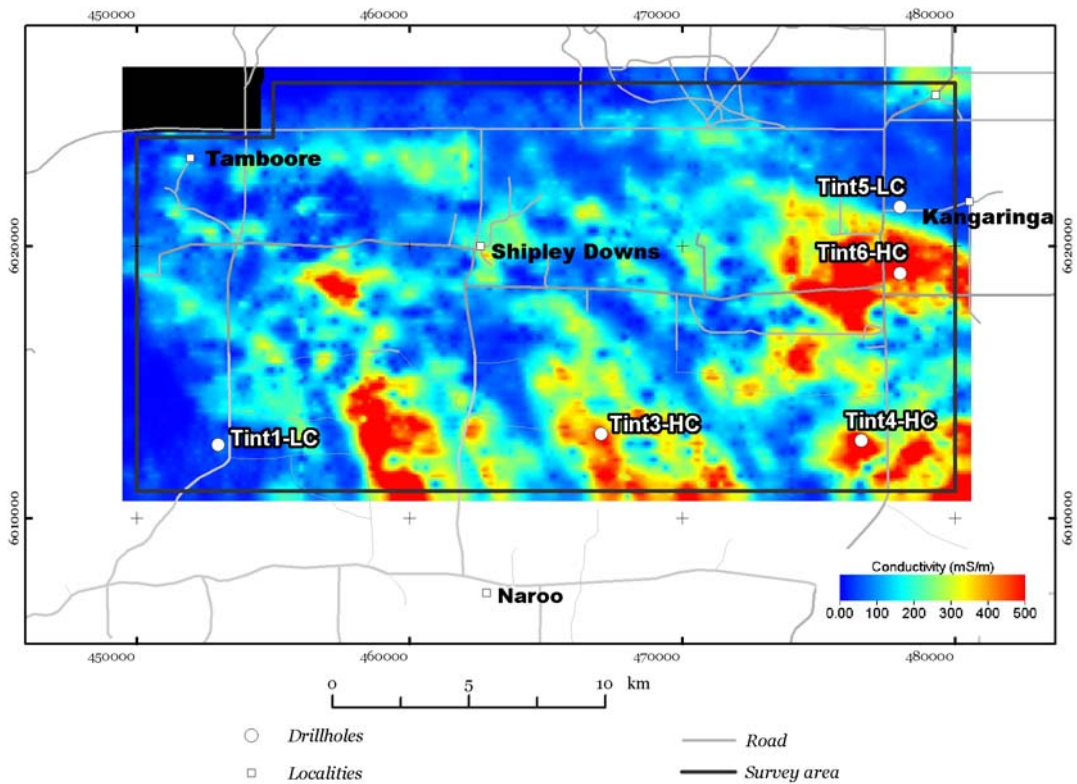


**Figure 4.** RESOLVE<sup>®</sup> HEM interval conductivity for 8-10 m below the surface, derived from a CDI transformation of those data. The locations of drill holes used to validate the observed conductivity structure are also shown.

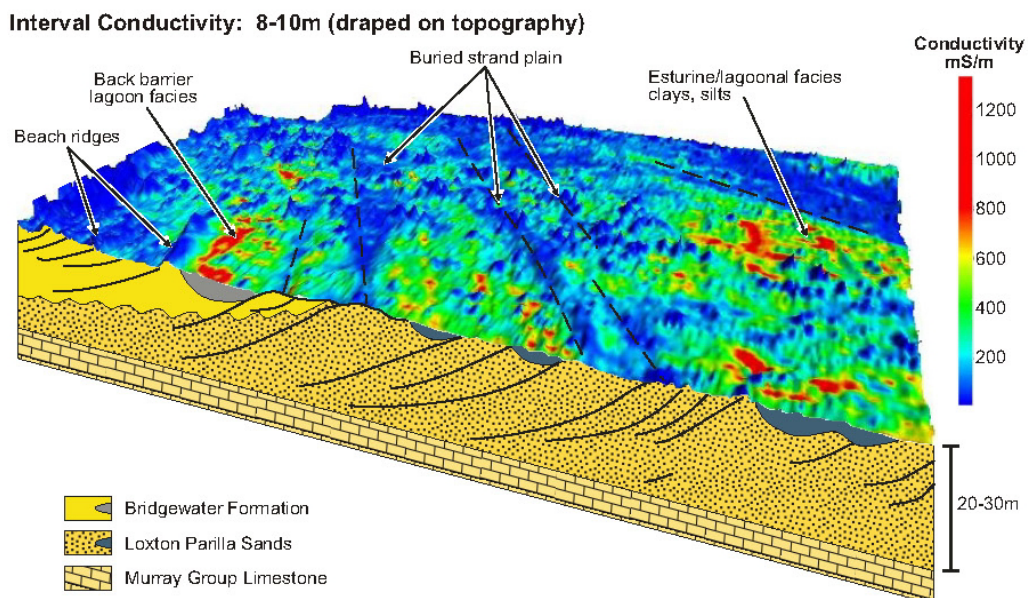


**Figure 5.** Block model of RESOLVE Interval conductivity for 8-10 m draped on topography, with a geological interpretation of the observed conductivity structure.

Although the RESOLVE<sup>®</sup> HEM system has a very wide bandwidth (106140 Hz to 385 Hz), it does not sample this frequency range in great detail. This under-sampling of the full frequency response means that it is difficult to invert these data to a complete vertical conductivity profile (Green *et al.*, 2003). However, it was clear that, for the Tintinara data set, it was not necessary to assume that *any* vertical conductivity profile was possible. Given the availability of information (from shallow bores in particular) about the distribution of conductive materials in this area and, because of the well-defined layering (a function of the sedimentary aquifer system) and well-characterized water table, it was possible to constrain the inversion of these data. This, in turn, meant that the restricted number of frequency measurements was no longer limiting the accuracy of interpretation. Using *a priori* information on the conductivity of Quaternary dune sands, the inter-dune clays, and the underlying Loxton-Parilla sands, derived from induction conductivity logs acquired in several bores across the area, along with knowledge of the depth to the groundwater and its conductivity, a four layer was defined to constrain the ID inversion. This is summarized in Table 1. The inversion was primarily directed at estimating the depth, thickness and conductivity of the near surface clay-rich sediments. The procedure adopted in the constrained inversion is described by Green *et al.* (2003).

**Table 1.** Initial assumptions about the conductivity structure in the Tintinara area.

|         |  |  |
|---------|--|--|
| Layer 1 | Recent sands                               | Non-conductive (~20 mS/m) Thickness variable between a few meters and 10m in isolated areas  |
| Layer 2 | Inter-dune/barrier clay sediments          | Conductive (average ~320 mS/m). Thickness: Usually a few meters, but variable, up to 30m in places. Absent on barrier systems.   |
| Layer 3 | Loxton-Parilla Sands above the water table | Non-conductive (~50 mS/m) Thickness: Variable depending on the water table. Typically 15-30 m.   |
| Layer 4 | Saturated Murray Group Limestones          | Conductive as determined by the porosity and the conductivity of the groundwater. Assumed to extend infinitely downwards Conductivity variable upwards from that of layer 5, |

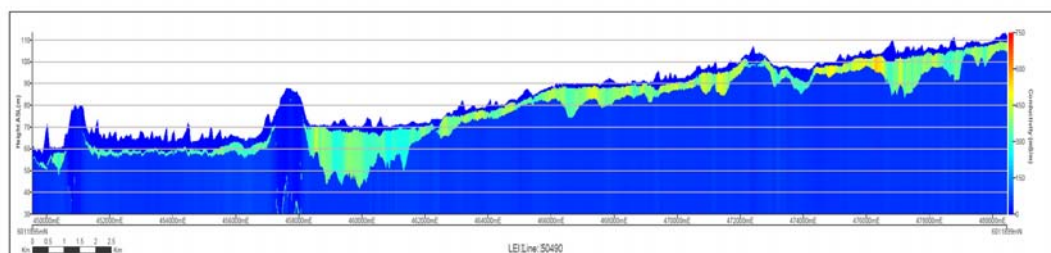


**Figure 6.** 1D Layered Earth conductivity depth section from the constrained inversion of one flight line. Clay rich sediments (the more conductive unit) are seen to occupy inter-barrier depressions and in places exceeds 30m in thickness.

Results from the constrained inversion of the HEM data suggest that clay rich sediments occupy the inter-barrier swales of the Loxton-Parilla sands in the east and Bridgewater Formation to the west. This is evidenced in the 1D LEI section (Figure 6) for a flight line transecting bores TIN-11C, 3HC and 4HC (see Figure 4 for their location). The stitched section indicates an irregular topography at the base of a conductive layer 2 (the clay rich sediments). In the east (right-hand side of the section) this relates to the beach strandline palaeo-topography which developed when

the Loxton-Parilla sands were deposited in the Early to Mid Pliocene. On the western (left) side of the section, the topography marks the base of the younger, carbonate rich sediments of the Bridgewater Formation which also developed as a progradational beach-barrier system.

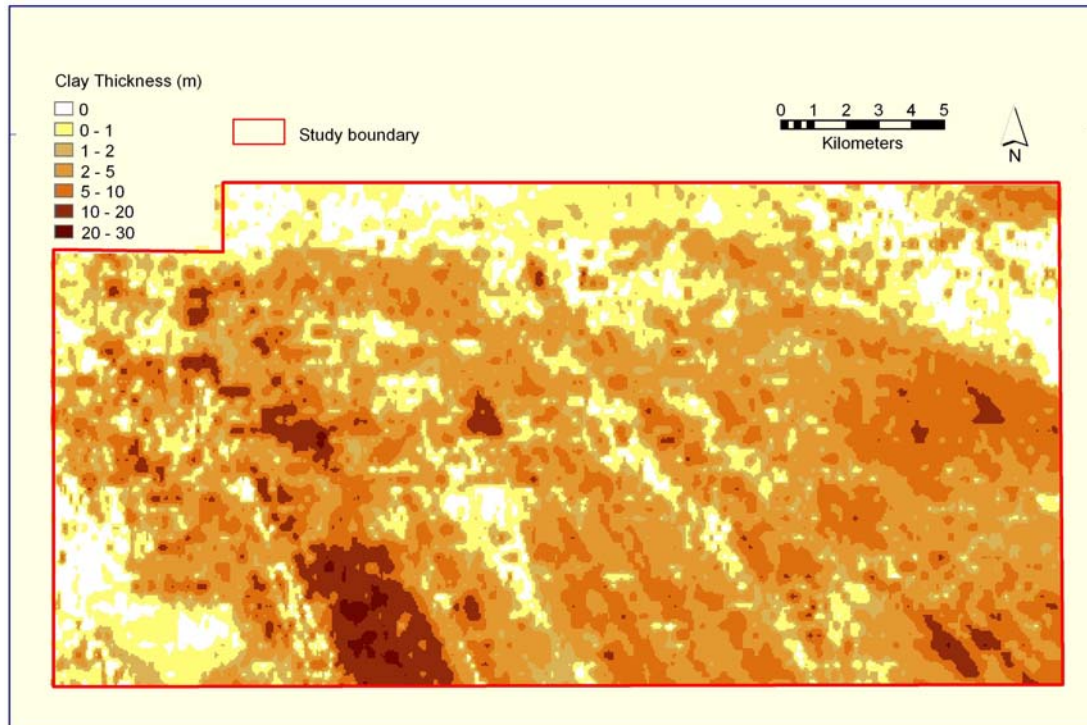


**Figure 7.** Map of the clay thickness derived from the constrained 1D LEI of RESOLVE HEM data. This is the direct equivalent to the thickness of Layer 2 in the inversion.

The 4-layer constrained inversion procedure nominally has nine parameters, three thicknesses and four conductivities. However because the conductivity of the lowest layer was held quite tightly to the value determined by the groundwater conductivity, this parameter was similar to the constraint data. Figure 7 shows a map of one of these parameters, the thickness of Layer 2 (Clay). This is the principal output from the application of the HEM data in this region, forming the basis for determining groundwater recharge rates or drainage flux in this part of the TCPWA. It will also be used to model the salt flux into the groundwater.

#### 4. GROUND VALIDATION AND TARGETED DRILLING

Five locations were selected for drilling (Table 2 and Figure 4) to validate the observed electrical conductivity (ECa) response. Borehole TIN1LC is situated towards the west of the survey area and targets an area with low ECa, whereas boreholes TIN3HC, TIN4HC and TIN6HC target high ECa areas. In comparison, borehole TIN5LC targets a low ECa in the northeast of the survey area.

**Table 2.** Table shows the boreholes coordinates and drill depths.

| <b>Boreholes</b> | <b>Easting (mE)</b> | <b>Northing (mN)</b> | <b>Depth (m)</b> |
|------------------|---------------------|----------------------|------------------|
| TIN1LC           | 453178              | 6012719              | 20               |
| TIN3HC           | 467050              | 6013100              | 22               |
| TIN4HC           | 476595              | 6012854              | 20               |
| TIN5LC           | 478000              | 6021450              | 23               |
| TIN6HC           | 478000              | 6019000              | 14               |

## 5. RESULTS

Several attributes, including sedimentary texture, water content, and petrophysical response (inductive conductivity and natural gamma), were determined. Leaney et. al. (1999) describe the methods of analysing for gravimetric water content and soil-water chloride (Cl). Results from these measurements are shown in Figures 8-12 (boreholes TIN-1LC, 3HC, 4HC, 5LC and 6HC respectively). Seven columns of data were displayed:

- The first column uses a schematic legend to summarise the main lithological units, eg. Molineaux-Lowan Sand, lagoonal Facies of, and Loxton-Parilla Sands. The second column provides comments on the lithology. The stratigraphic units have been defined and described in Brown and Stephenson (1991).
- The third column shows the particle size distribution as sand, silt and clay percentages.
- The fourth column shows the gravimetric water content of individual samples, with ½ to 1 m composites.
- The fifth column shows the soil-water chloride results.
- The sixth column displays the down-hole apparent electrical conductivity (ECa) measured by an induction logging tool.
- The seventh column shows the down-hole natural gamma log. The response is the composite of emissions from three radioelements K, U and Th and their daughter isotopes.

### 5.1. Borehole TIN1LC

Borehole TIN1LC was drilled on the foot slope of a dune. The surface 2 m of loose fine sandy soil is interpreted as Molineaux-Lowan Sands. This is followed by 18 m of interbedded light brown, fine quartz sand and calcareous muddy sand. The unit becomes coarser and calcareous with depth, with an increase in abundance of moderately sorted fine to medium calcareous sand. This unit is interpreted as the Bridgewater Formation. Drilling stopped at 20 m when a hard (cemented?) unit was encountered with no sample returned.

The overall electrical conductivity response is low (<100 to 200 mS/m) with a slight elevation between 3 to 6 m associated with an increase in water content (0.2 g/g). The chloride concentrations remain low for the top 6 m and increases gradually with depth (up to 10,000 mg/l at the highest concentration at 9.5 m). The presence of clay and silt fractions in the visual display is due to fine-grained calcite, commonly occurs as coatings on quartz sand. XRD results show that no phyllosilicate mineral (eg. kaolinite or smectite) is present.

### 5.2. Borehole TIN3HC

Borehole TIN3HC was drilled in a ploughed field and intersected 15 metres of dominantly grey, fine sandy clay and sandy mud with white limestone beds, interpreted as the back-strand lagoonal facies of the Loxton-Parilla Sands. Underlying is at least 7 m of yellow to light brown, fine to medium, well to moderately sorted sand, interpreted to be the Loxton-Parilla Sands.

The lagoonal facies of the Loxton-Parilla Sands is sand-rich towards the base, grading upwards to massive white fine-grained (partly cemented) calcite (7.5 to 11 m depths), and increases in clay and silt abundance (smectite and kaolinite-rich) in the upper part of the unit. The soil (top 2 m) developed within this formation comprises muddy sand. Varying abundance of white calcite

concretions is present throughout the formation. This lagoonal facies overlies well sorted fine quartz sand (Loxton-Parilla Sands).

Changes in the textures and mineral composition of the unit are also reflected in the water contents and electrical conductivities. Both the water contents and electrical conductivities are high in the top 7.5 m, associated with high clay content, and decrease towards the base of the formation. The gradual increase in chloride concentrations down the profile could not offset the decrease in conductivity caused by the decreasing water content. In the Loxton-Parilla Sands, both the water contents and electrical conductivities remain low.

The down-hole gamma signature may be divided into 2 sections, an upper section (1 – 7.5 m) with higher gamma values corresponding to the silt-rich beds, and a lower section (7.5 – 19 m) with lower gamma values corresponding to the calcite and sand-rich beds.

### **5.3. Borehole TIN4HC**

Borehole TIN4HC was drilled on a sand plain cleared of native vegetation. The interpreted lithology present includes Molineaux-Lowan Sands, lagoonal facies of the Loxton-Parilla Sands, and the Loxton-Parilla Sands. The unit descriptions are as follows.

The Molineaux-Lowan Sands comprise 2 m of moderately sorted fine to medium sand and poorly sorted fine to coarse sand and muddy sand. Quartz is the dominant mineral with minor kaolinite.

The lagoonal facies comprises of 12 m (*i.e.* 2 to 14 m depth) of grey mottled sandy clay and sandy mud with minor beds of yellow-brown muddy sand and sand. Local cemented carbonate concretions are present throughout. The mineral composition includes, depending on textures, varying proportion of quartz and smectite, and less abundant mica (illite/muscovite) and kaolinite. The sandy clay with carbonate concretions contains significant quartz and calcite, and the coarse sand fraction is attributed to cemented calcite grains.

The Loxton-Parilla Sands consist of at least 6 m of yellow to yellow brown, well to moderately sorted, fine to medium sand and comprise dominantly of quartz with minor K-feldspar.

The conductivity throughout the lithologic units range from 100 mS/m to 600 mS/m, and the profile shows two ‘bulges’. The first is present from 2 to 7 m and the second from 11 to 15 m. Since the chloride concentrations remain fairly consistent (10,000 to 13,000 mg/l) down the profile, the attributes that drive the electrical conductivity response appears to be the texture (clay) and the associated higher water content (0.15 to 0.25 g/g). Hence, both conductivity bulges are associated with an increase in clay and silt content in the lagoonal facies, coupled with an increase in water content.

The natural gamma log shows a decrease in response from the Molineaux-Lowan Sands down to the base of the lagoonal facies, and remains low in the Loxton-Parilla Sands.

### **5.4. Borehole TIN5LC**

Borehole TIN5LC was drilled on a sand plain and intersected 3.5 m of unconsolidated fine sand with clean quartz. This unit is interpreted as the aeolian Molineaux-Lowan Sands. A thin layer of cemented sand (5 cm) at the base of the Molineaux-Lowan Sands caused a local perched fresh

water lens, evidenced from a higher water content (0.2 g/g) coupled with a low chloride concentrations (< 100 mg/l). Underlying is 20 m of massive, compact, leached (very pale grey) to light grey, mottled, moderately sorted fine to medium sand. Minor silt-rich beds are present locally. This unit is interpreted to be the Loxton-Parilla Sands. Quartz is the dominant mineral in both lithologic units with minor kaolinite and mica.

The conductivity and gamma logs stopped at 15 m due to hole collapse. The electrical conductivity remains low (100 – 200 mS/m) throughout the profile, with slightly elevated conductivity associated with an increase in water content (eg. 7-8 m). This increase in water content is attributed to an increase in abundance of very fine silt. The local perched fresh water (2 - 4 m) does not give high conductivity response (50 – 100 mS/m).

### **5.5. Borehole TIN6HC**

Borehole TIN6HC was located on a sand plain and the interpreted lithology present includes Molineaux-Lowan Sands, back-strand lagoonal facies of the Loxton-Parilla Sands, and Loxton-Parilla Sands. A brief description of the individual lithology is as follows.

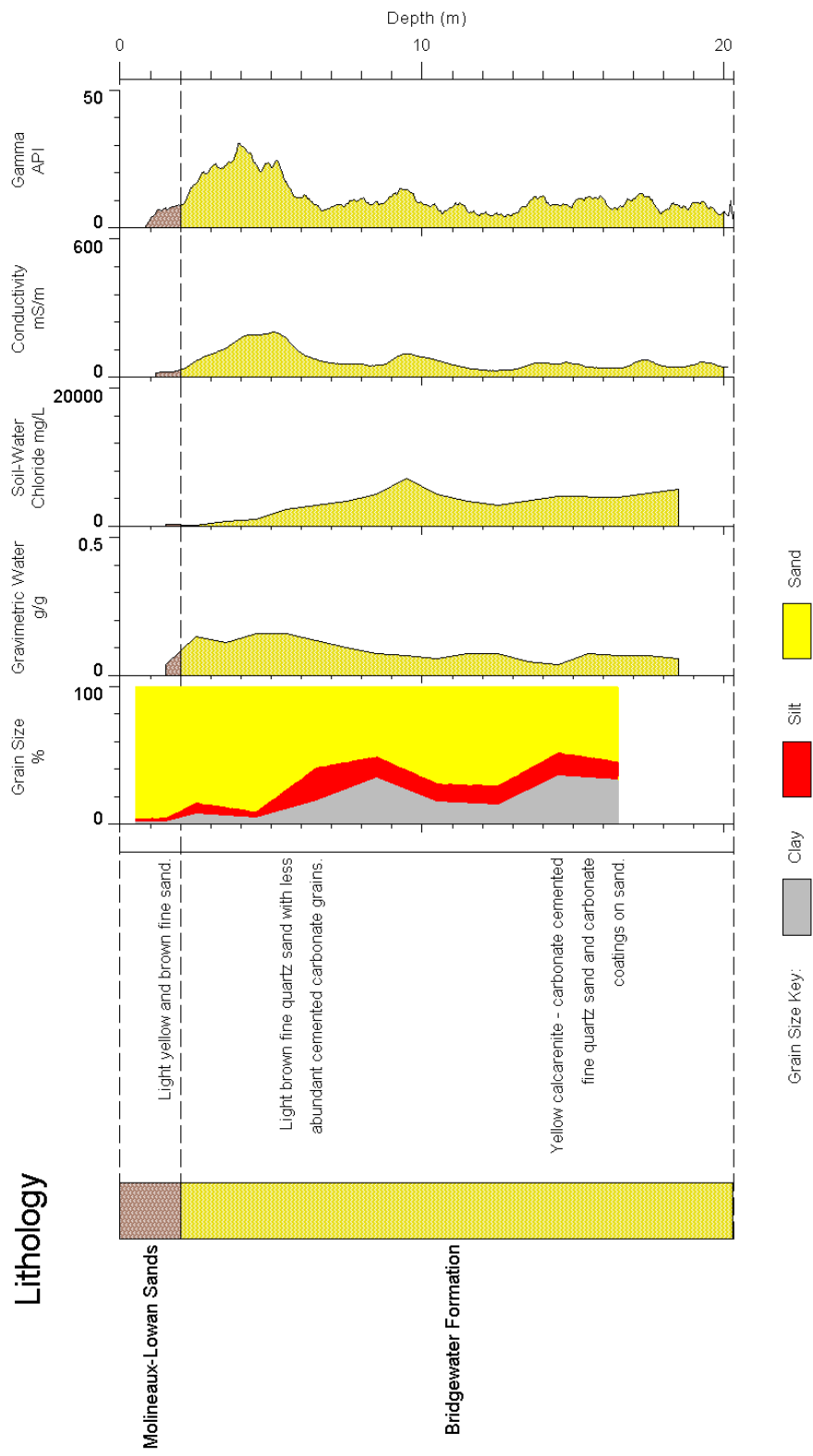
The Molineaux-Lowan Sands comprise 3 m of yellow to yellow-brown, loose, fine to medium sand with abundant organic matter present in the top metre. The underlying lagoonal facies consists of 9.5 m of yellow and grey-mottled sandy clay and sandy mud, with 1.5 m of pale grey muddy sand layer present at the base of the unit (11-12.5 m). Cemented concretions or powdery carbonate are present locally in the upper part of the Formation. Underlying is at least 2 m of massive, compact, yellow and pale grey, moderately sorted medium sand of the Loxton-Parilla Sands.

Results from grain size analysis show that the Molineaux-Lowan Sands is sand-rich, whereas the lagoonal facies is clay and mud-rich, except at the base where sand is present. The Loxton-Parilla Sands is sand-rich, with very little clay and silt. The mineral composition of the Molineaux-Lowan Sands and Loxton-Parilla Sands comprises essentially of quartz. The lagoonal facies sediments consist of quartz, calcite, and varying abundance of smectite, illite and kaolinite. No clay mineral is present in the white calcite bed from 4 to 5 m, and the abundant silt fraction is attributed to the fine-grained calcite.

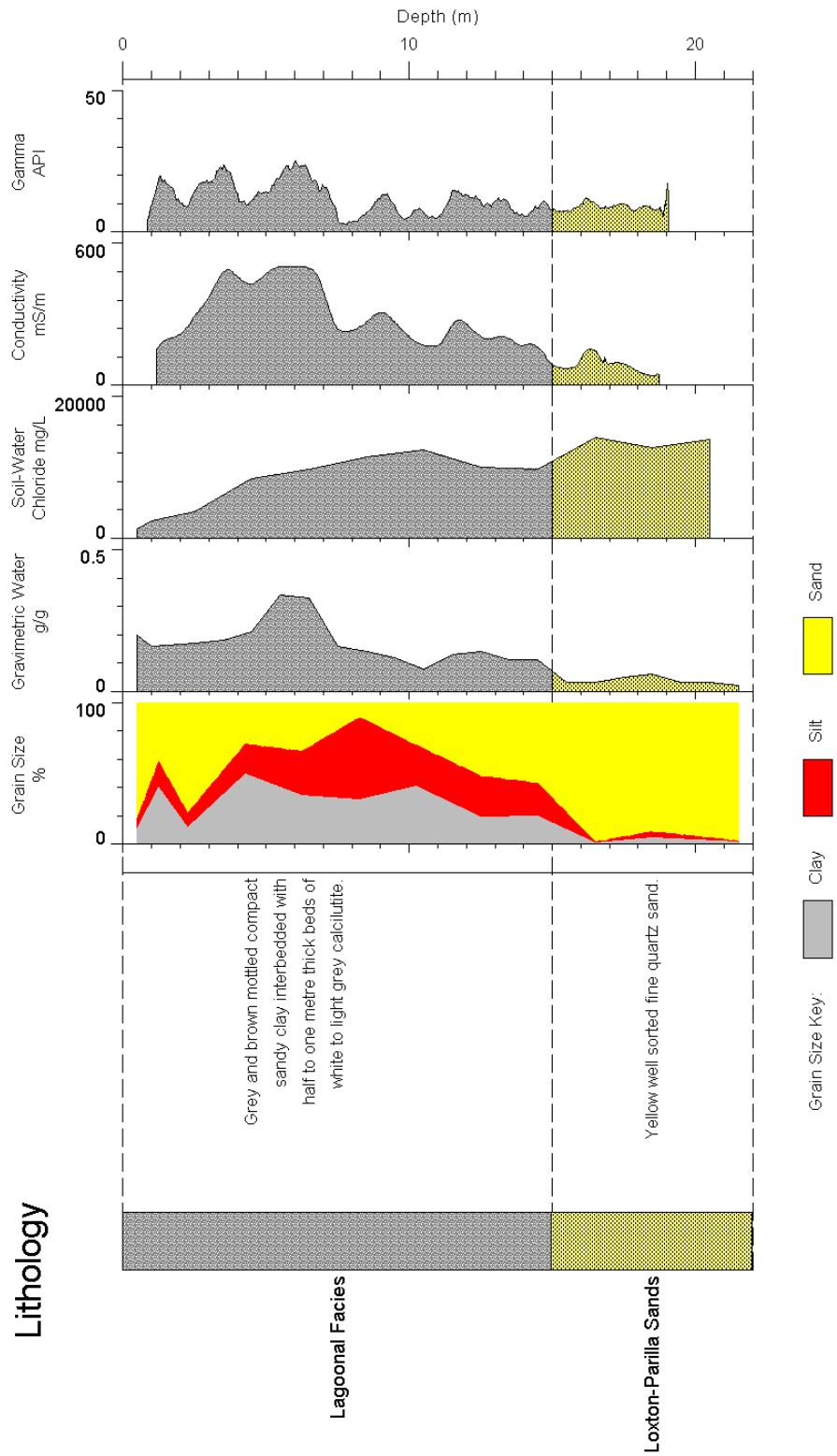
The water content is associated with the grain size distribution, and started with low water content (0.1 g/g) in the Molineaux-Lowan Sands, and increases (0.2 – 0.35 g/g) towards the base of the lagoonal facies associated with high silt content. The water contents decrease (0.1 g/g) across the disconformity to the underlying Loxton-Parilla Sands. The soil-water chloride content is low (1,000 mg/l) within the first metre of the Molineaux-Lowan Sands, but increases significantly (10,000 mg/l) towards the base, and remains high in the lagoonal facies (10,000 to 14,000 mg/l).

The down-hole electrical conductivity trend mimics the distribution of clay abundance and the associated water content. The conductivity is low to moderate in the Molineaux-Lowan Sands (200-300 mS/m), increases in the lagoonal facies (500-600 mS/m), but decreases at the base of the lagoonal facies in the presence of basal clayey sand. No data is available in the Loxton-Parilla Sands as the sand collapsed.

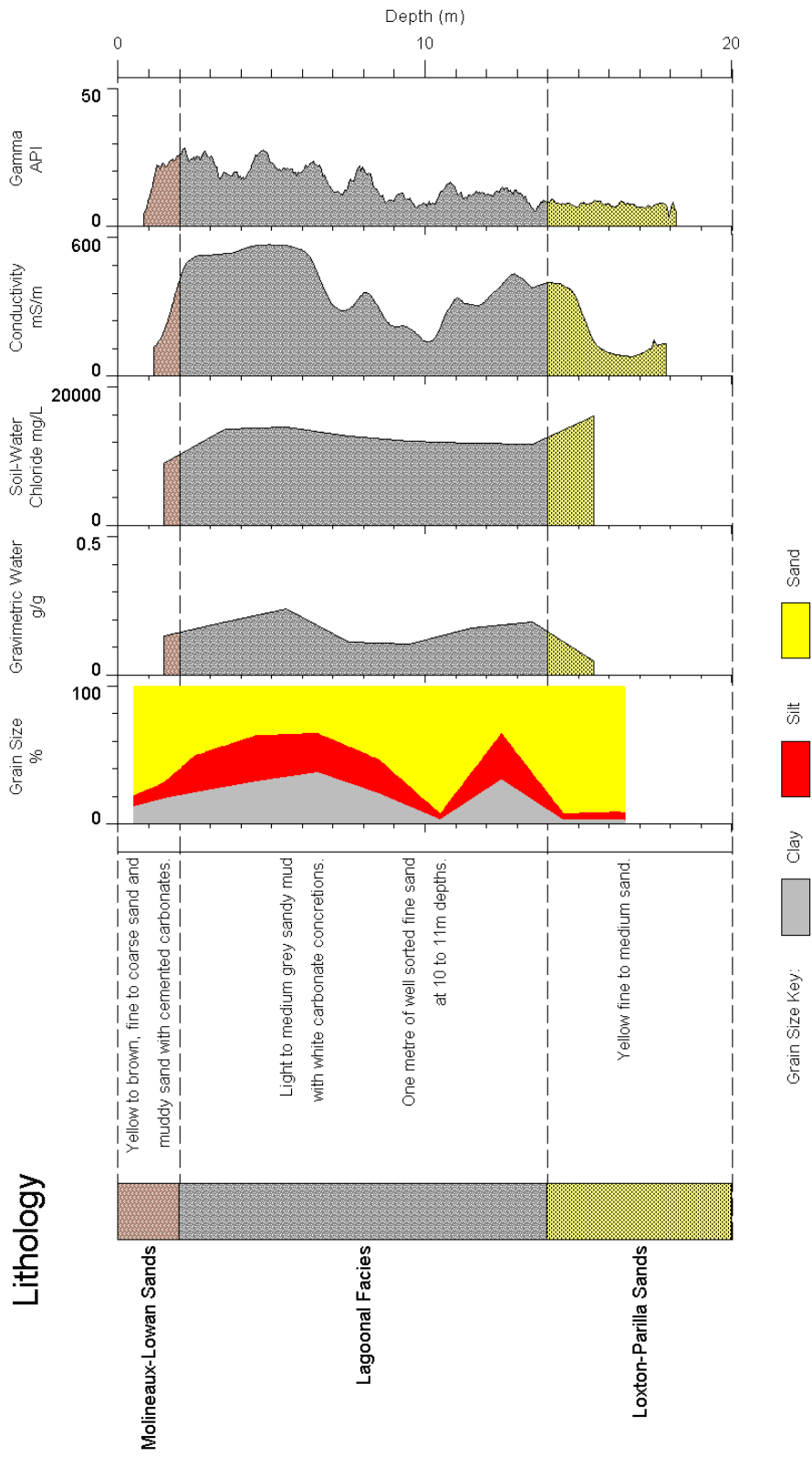
# Bore TIN1LC



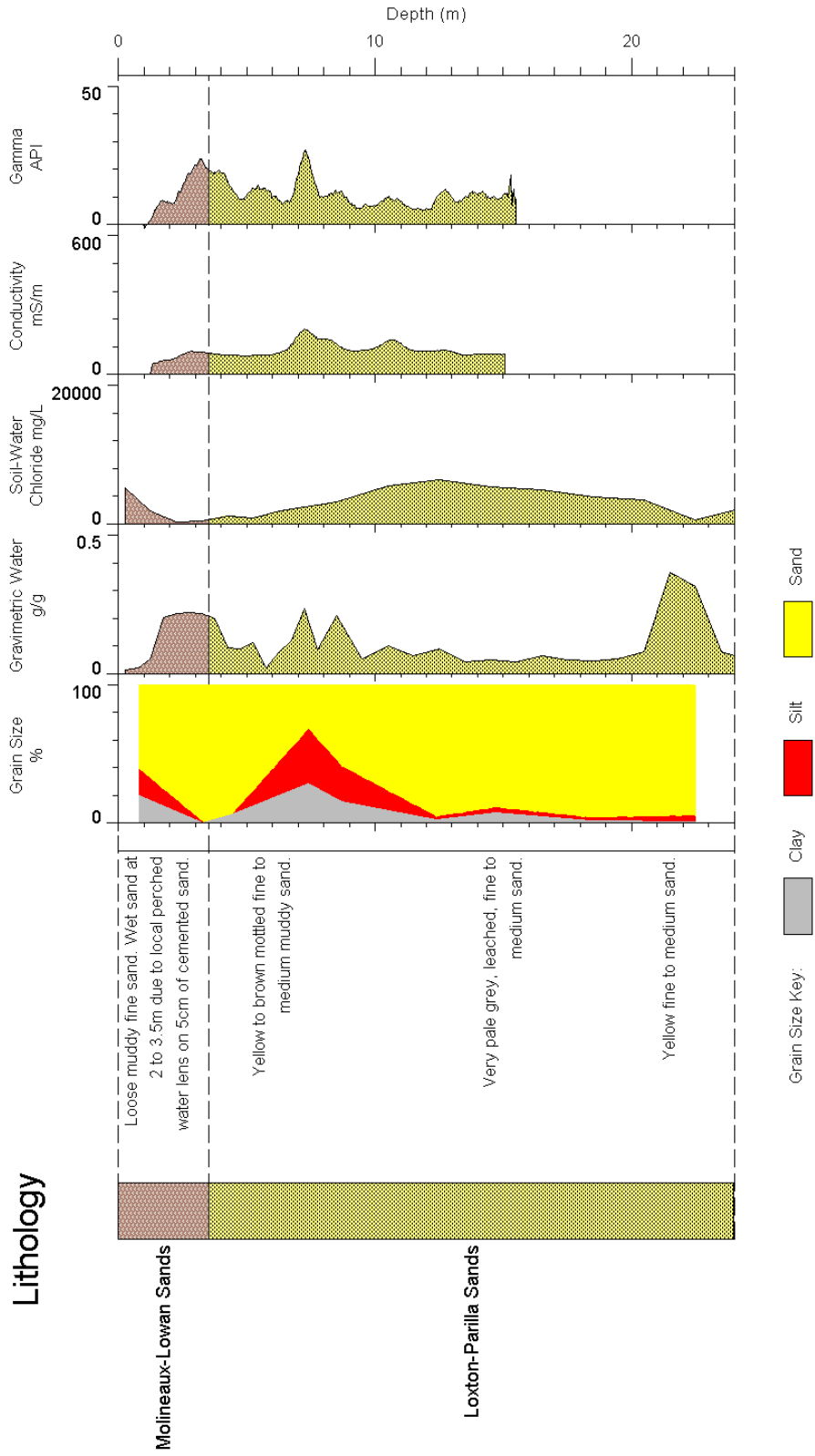
# Bore TIN3HC



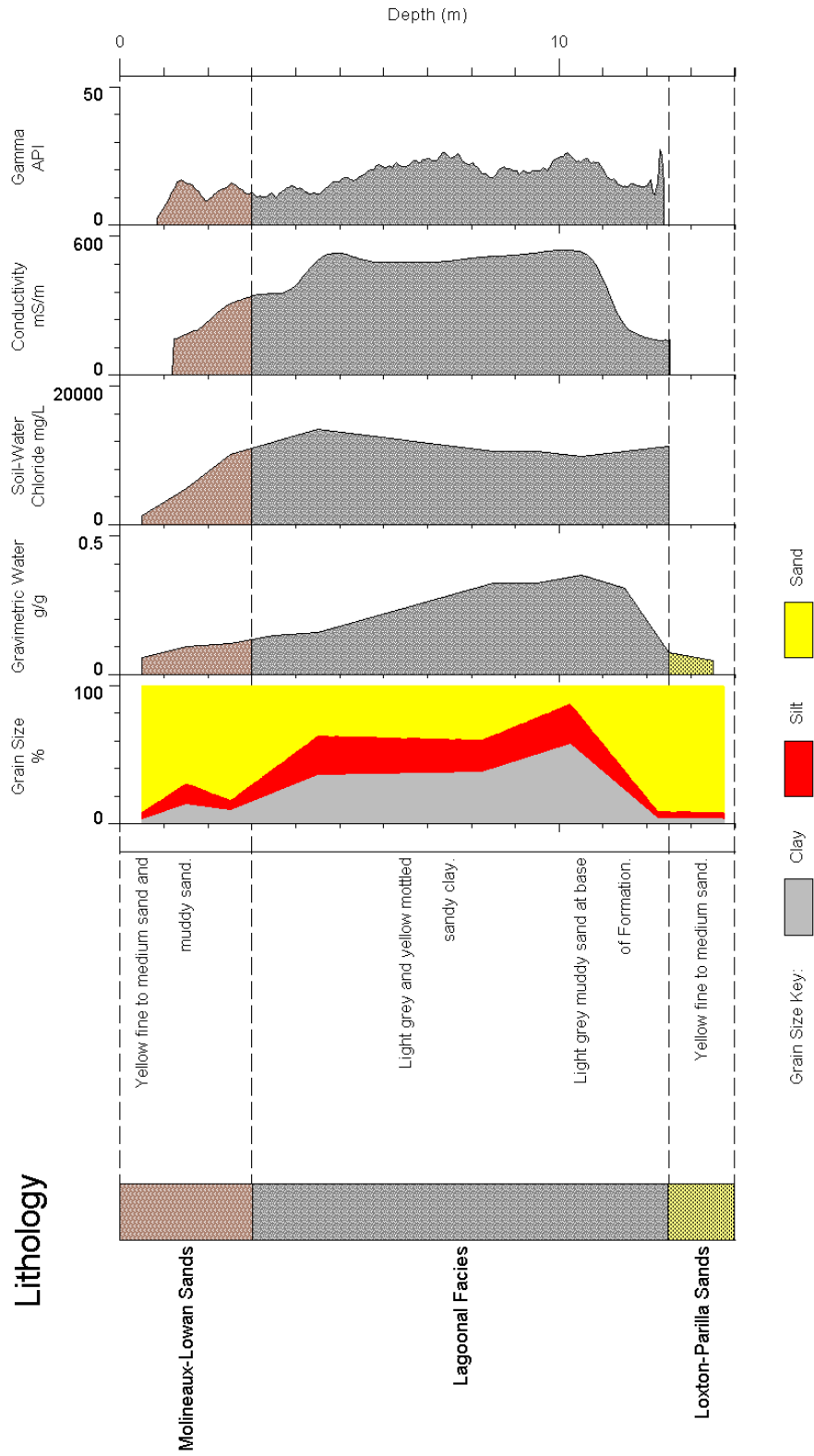
# Bore TIN4HC



# Bore TIN5LC



# Bore TIN6HC



## 5.6 Petrophysical Attributes

### 5.6.1 Water Content

The water content shows skewed population (Figure 13a), with the modal class between 5 and 10 wt. %. Grouping the data into the respective lithologic units reveals that the Loxton-Parilla Sands exhibit the lowest range (median 5 wt. %), whereas the lagoonal sediments have the highest water content (median 16.5 wt. %) (Figure 13b). In comparison, both Molineaux-Lowan Sands and Bridgewater Formation have low to moderate water contents (median of 6 and 9 wt. % respectively).

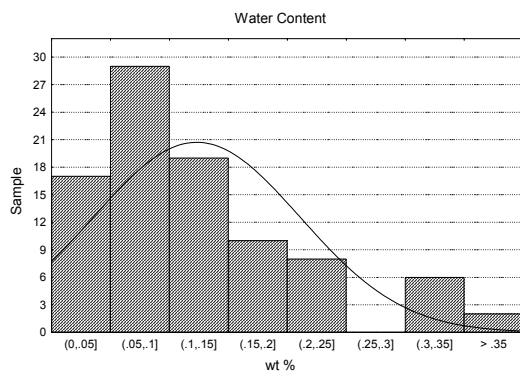


**Figure 13a.**  
The water content distribution shows a skewed population.

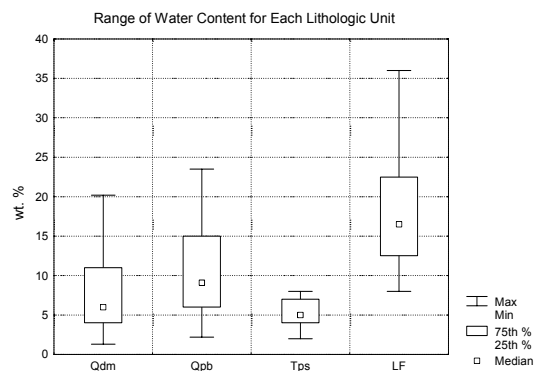


**Figure 13b.**  
Range of water content for each lithologic unit.  
**Legend:**  
Qdm – Molineaux-Lowan Sands  
Qpb – Bridgewater Formation  
Tps – Loxton-Parilla Sands  
LF – lagoonal facies

### 5.6.2 Chloride Concentration

The distribution of pore water chloride concentrations comprises two populations. The first population falls below 6000 mg/l and the second population is greater than 8,000 mg/l (Figure 14a). All the lithologic units, except the lagoonal facies sediments (median of 10,800 mg/l), have median values below 6,000 mg/l (Figure 14b). Nevertheless, the Loxton-Parilla Sands exhibit the largest variance of chloride concentrations, ranging from relatively fresh (200 mg/l) to saline (15,800 mg/l).

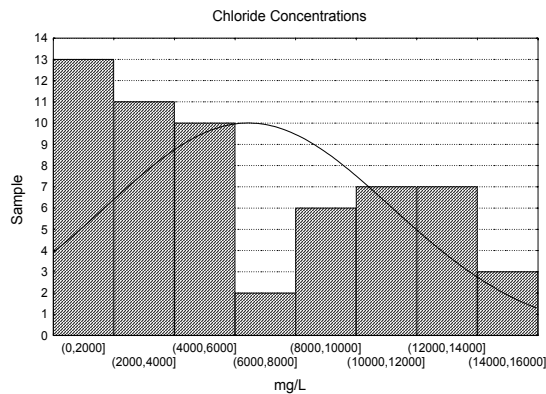


**Figure 14a.**

The distribution of chloride concentrations comprises two populations. The first population is < 6000 mg/l and the second population is > 8,000 mg/l.

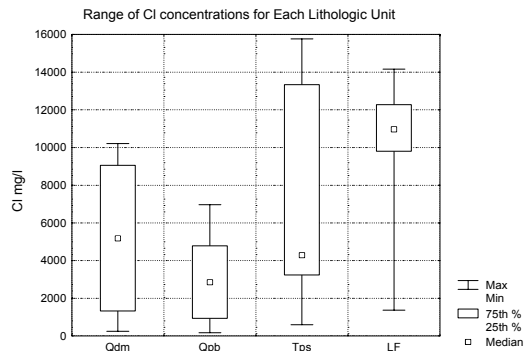


**Figure 14b.**

Range of chloride concentrations showing wide range for the Loxton-Parilla Sands.

**Legend:**

**Qdm – Molineaux-Lowan Sands**

**Qpb – Bridgewater Formation**

**Tps – Loxton-Parilla Sands**

**LF – lagoonal facies**

### 5.6.3 Grain Size Distribution, Clay Abundance and Mineralogy

The grain size distribution shows two populations of clay abundances. The first population ranges from 5 to 25 vol. % whereas the second population ranges from 25 to 60 vol. % (Figure 15a). The median value (3 vol. %) of the Loxton-Parilla Sands falls within the modal class (0-5 vol. %) of the first population (Figure 15b), and the median values (11 and 17 vol. % respectively) of the Molineaux-Lowan Sands and the Bridgewater Formation, albeit higher, also belongs to the first population. In contrast, the median value (32 vol. %) of the lagoonal Facies sediments falls within the second population. The dominant textures of the combined sedimentary units are sand, muddy sand and sandy mud, and less abundant in sandy silt and sandy clay (Figure 15c). Amongst these textures, the lagoonal facies sediments comprise dominantly of sandy mud and sandy clay, with minor sand beds.

The main phyllosilicate mineral that made up the clay fractions is kaolinite, with smectite and mica (illite/muscovite) present in some samples. Although the Bridgewater Formation (bore TIN1LC) may contain relatively high abundance of clay fraction, this fine texture is attributed to calcite, as phyllosilicate minerals are absent.

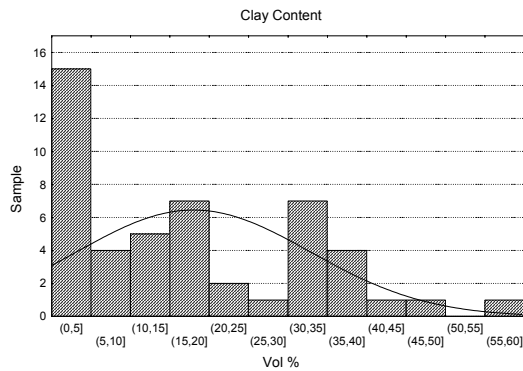


**Figure 15a.** Histogram distribution of clay abundance. Two populations are present, the first ranges from 0 to 25 vol. %, and the second ranges from 25 to 60 vol. %.

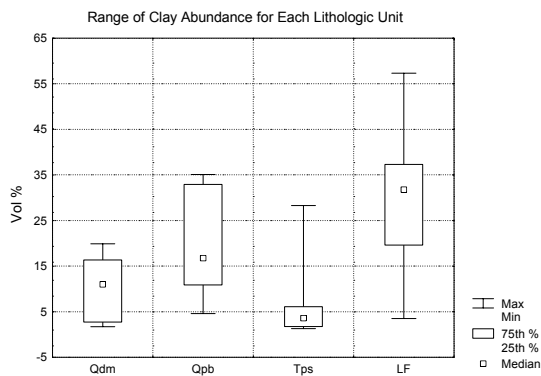


**Figure 15b.** Range of Clay vol % for each lithologic unit. The Clay contents of Bridgewater Formation are attributed to fine-grained carbonates and not phyllosilicates (e.g. kaolinite).  
**Legend:**  
**Qdm** – Molineaux-Lowan Sands  
**Qpb** – Bridgewater Formation  
**Tps** – Loxton-Parilla Sands  
**LF** – lagoonal facies

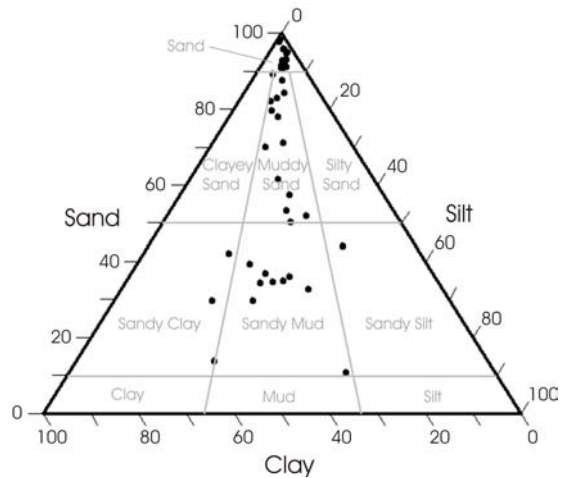


**Figure 15c.** Ternary diagram of sand, silt and clay volume % using the sedimentary classification system (Lewis and McConchie, 1994). The sedimentary textures comprise dominantly of sand, muddy sand and sandy mud, with fewer sandy silt and sandy clay. The sandy mud and sandy clay are mostly lagoonal facies sediments.

### 5.6.4 Electrical Conductivity

The electrical conductivity shows two populations, the first ranges from 0 to 300 mS/m, with modal class of 50 to 100 mS/m, whereas the second population ranges from 300 to 600 mS/m, with modal class from 500 to 550 mS/m (Figure 16a). The median values of Lowan-Molineaux Sands, Bridgewater Formation and Loxton-Parilla Sands belong to the first population (Figure 16b), but there are large variances for the latter two units, with conductivity values up to 400 mS/m. The lagoonal facies sediments have the highest median (380 mS/m), with maximum conductivity of 570 mS/m, and the 25<sup>th</sup> percentile at 240 mS/m. However, this unit also comprises low conductivity values (eg. 100 mS/m). Nevertheless, these results suggest that the conductive areas shown in the inversion products from the AEM data are attributed to the lagoonal facies sediments (of the Loxton-Parilla Sands), whereas the resistive areas comprise the other three

dominantly resistive lithologic units. The 25<sup>th</sup> percentile for the lagoonal facies (*i.e.* 240 mS/m) can be used as a threshold value in differentiating between conductive and resistive sediments in the study area.

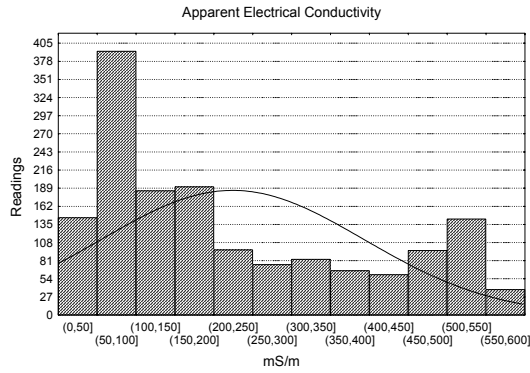


**Figure 16a.**  
The electrical conductivity shows two populations, the first is less than 300 mS/m and the second population ranges from 300 to 600 mS/m.

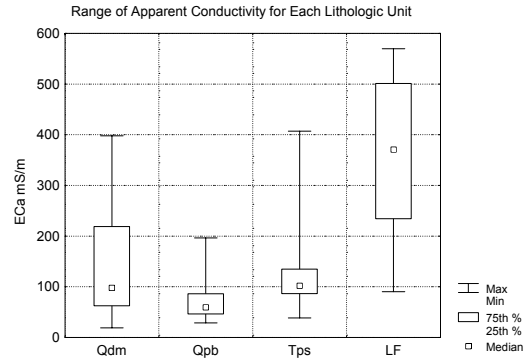


**Figure 16b.**  
Range of electrical conductivity values showing the lagoonal Facies sediments having the highest median.

**Legend:**

**Qdm – Molineaux-Lowan Sands**

**Qpb – Bridgewater Formation**

**Tps – Loxton-Parilla Sands**

**LF – lagoonal facies**

## 6. DISCUSSION

This section examines the petrophysical attributes (*i.e.* the electrical conductivity, water content, pore water salinity, and clay abundance) of the sediments found in the study area to determine the principal factors driving the observed electrical conductivity. The intent is to verify the use of electrical conductivity to map the distribution of mud and clay-rich sediments. The validation and interpretation of the near surface conductivity depth interval data is also discussed, as is the veracity of the constrained inversion product (*i.e.* the thickness of layer 2 image), which is cross referenced against borehole information to provide new insight into the sedimentary framework in the AEM survey area.

### 6.1. Causal Relations amongst the Petrophysical Attributes

Rhoades et al. (1976) demonstrated that the apparent conductivity is the weighed summation of electrical conductivities of liquid and solid phases (Equation 1). In the absence of massive sulphides, conductivity is attributed to the liquid phase, which is in turn driven by the volumetric water content and the electrolyte (mainly sodium and chloride) ion concentrations of the pore water.

$$ECa = ECw\theta\tau + ECs \quad \text{Equation 1}$$

where  $ECa$  is the apparent conductivity,  $ECw$  is the pore water conductivity,  $\theta$  is the volumetric water content,  $\tau$  is the tortuosity and  $ECs$  is the solid phase conductivity.

To avoid ambiguity in interpreting the electrical conductivity and its attributes, carbonates samples are not included in the analyses that follow. The term ‘clay’ is used to describe less than 4  $\mu\text{m}$  fractions that comprise phyllosilicate minerals only.

The water holding capacity is a function of a materials’ porosity and generally increases from coarse to fine textured materials (Brady, 1990). A graph of water content against clay abundance (Figure 17a) reveals that the water content is positively associated with clay abundance. However, a spread of data points suggests that the water contents vary considerably amongst similar textured materials, e.g. sand may be relatively dry (< 5 wt. %) or wet (up to 17 wt. %). Likewise, the mud (*i.e.* 30-40 vol. % clay) also contains varying amounts of water contents, *i.e.* between 12 to 33 wt. %. Such variations in water contents within each textural class have significant influence on the correlation between the electrical conductivity and clay abundance, as elaborated below.

The plot of electrical conductivity against water content shows only a weak positive correlation with a large spread of data. However, grouping the data into three classes according to chloride concentrations reveals stronger relationships (Figure 17b). This suggests that when the pore fluid salinity is held relatively constant, the apparent electrical conductivity is positively correlated to the water content.

The amount (mass) of saline pore water in a given unit (mass) of sediments is termed salt load. Total salt loads can be calculated by multiplying the sample water content with the sum of major cations and anions concentration. A plot of electrical conductivity against salt load (mg/kg chloride) shows a good correlation between the two ( $r = 0.89$ ) (Figure 17c). Equation 1 would suggest that an increase in salt load would lead to an increase in the electrical conductivity of the liquid phase and a rise in the overall electrical conductivity.

The relationship between electrical conductivity and clay abundance shows wide spread distribution of data that results in a moderate, but positive, correlation ( $r = 0.65$ ) (Figure 17d). Grouping the data into their water contents revealed that the absence of a strong relationship is partly attributed to the variations in water contents within each textural class (also shown in Figure 17a). Overall, three outlier groups (Groups A, B and C) are observed, with the conductivities for Groups A and B being higher than those sediments with similar clay abundance (Figure 17e). An improved correlation ( $r = 0.91$ ) is achieved by omitting these outliers. Since the electrical conductivity is a measure of the salt load, the regression line ( $y = 7.4x + 62$ ) in Figure 17e denotes a proportionate increase in salt load with respect to clay abundance. The presence of the outlier groups however, reflects that the salt loads for these samples are not in proportion with the texture.

Since salt load is a function of water content and pore fluid salinity, groups A and B represent samples containing higher water contents than the other samples with similar clay abundance (texture) that are closer to the regression line. On the other hand, data in Groups B and C have similar water contents (15 – 36 wt. %), but the latter, Group C, is below the regression line as a result of lower pore fluid salinity.

The primary driving factor influencing electrical conductivity is salt load, which is a function (product) of water content and its salinity. Small variation in water content of materials with similar texture and consistent pore fluid salinity will result in a strong and positive correlation between the electrical conductivity and clay abundance. On the other hand, larger variations in water contents and / or pore fluid salinity result in a weaker correlation, with wide spread of data, *i.e.* outlier populations that plot away from the regression line. Under such circumstances, an increase in salt load / electrical conductivity is not accompanied by a proportionate increase in clay abundance.

From the statistical analyses, the threshold of 240 mS/m can be used arbitrarily to separate between more conductive and more resistive sediments. From the aforementioned line of regression, 240 mS/m will equate to approximately 24 vol. % clay. The sedimentary texture ternary diagram indicates that samples containing more than 24 vol. % clay comprise sandy mud and sandy clay. Since the sands (*i.e.* muddy sand and sand) are dominantly resistive with only a handful of wet and conductive saline sand, a map of electrical conductivity could be used to map the conductive mud and clay.

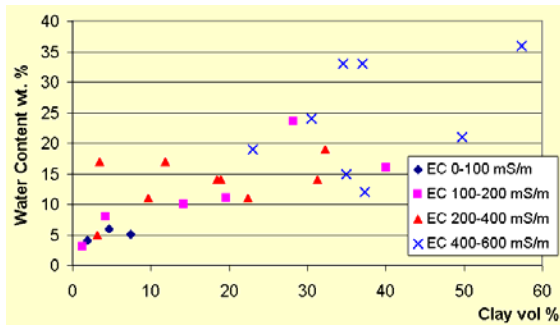


**Figure 17a.**  
Scatter plot shows positive correlation between water contents and clay abundance.

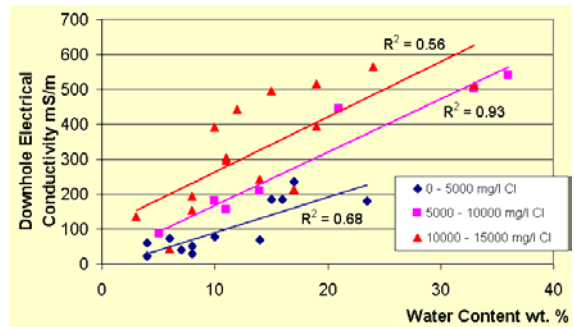


**Figure 17b.**  
Positive correlation of electrical conductivity and water content with respect to the three classes of chloride concentrations.

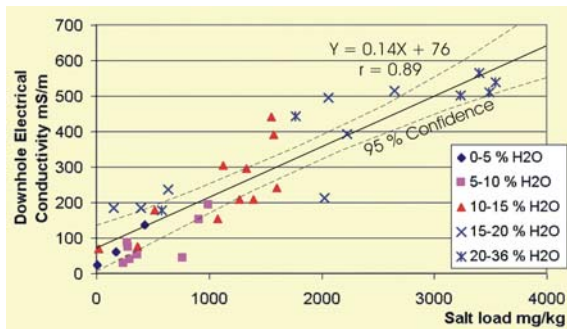


**Figure 17c.**  
Positive correlation between electrical conductivity and salt load (mg/kg chloride), suggesting the main factors driving EC are water contents and pore water salinity.

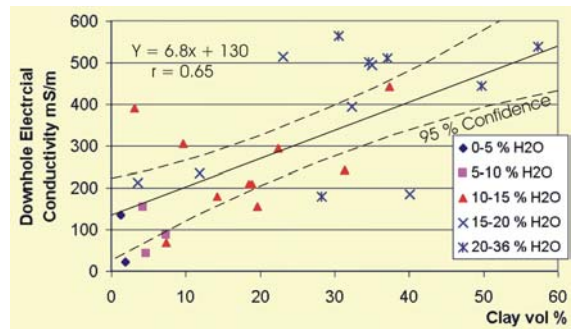


**Figure 17d.**  
Weak, but positive correlation of electrical conductivity with clay abundance. The data was grouped according to the water contents.

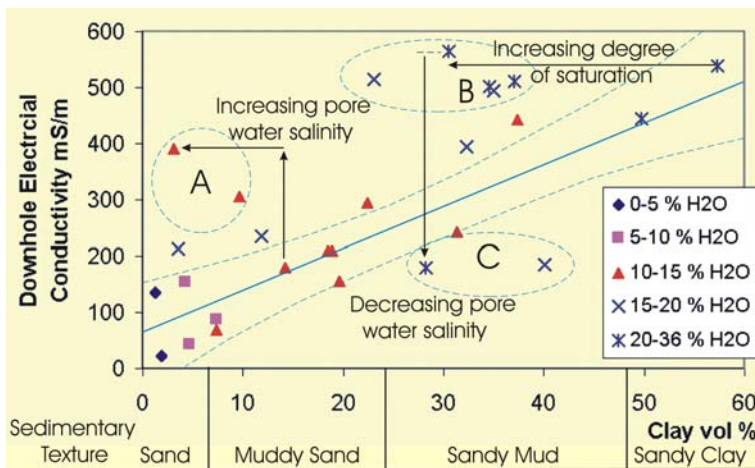


**Figure 17e.**  
Scatter plot is the same as Figure 14d with outlier Groups A, B and C delineated. Improved correlation of  $r = 0.91$  when Groups A, B and C are omitted. The regression line ( $y = 7.4x + 62$ ) denotes constant increase in salt load associated with a proportionate increase in clay abundance.

## 6.2 Validation and Interpretation of CDI image

With the geo-electrical characteristics of individual lithologic units defined, and the relationship between conductivity and clay abundance established, the CDI images can be interpreted with greater confidence.

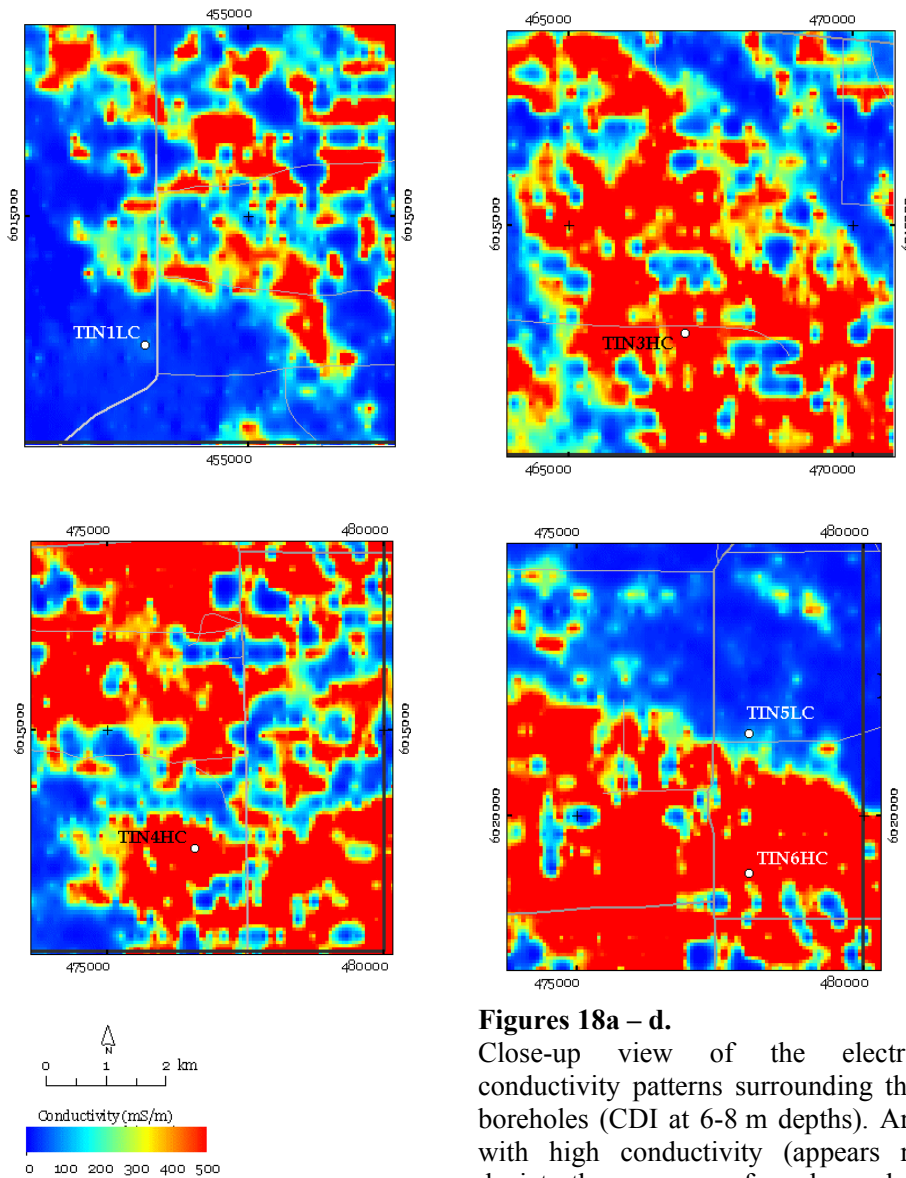
Five boreholes were selected to target various electrical conductivity responses as shown, for example in the 6-8m conductivity-depth interval image (Figure. 15a – d). The surficial Molineaux-Lowan Sand, commonly 2 to 3 m thick, would not be represented in this depth interval. The other lithologic units, along with their average conductivity between 6-8 m (from down-hole conductivity logs) are shown in Table 4, and the results concur with the conductivity values shown on the CDI image (Fig. 18a-d).

Boreholes TIN3HC, TIN4HC and TIN6HC target areas with high conductivities ( $> 350$  mS/m), whereas boreholes TIN1LC and TIN5LC target areas with low conductivities ( $< 150$  mS/m). Results from the correlation of electrical conductivity and clay, and the box plots of the range and percentiles of lithologic electrical conductivity, suggests 240 mS/m is the threshold for separating sands from mud and clay. Therefore, the broad conductive patterns surrounding boreholes TIN3HC, TIN4HC and TIN6HC are interpreted as consisting of conductive sandy mud ( $> 24$  vol. % clay) and sandy clay ( $> 49$  vol. % clay), and are linked to the back-barrier lagoonal facies, with minor inter-bedded, conductive wet saline sands.

The low conductive areas ( $< 150$  mS/m) shown on the CDI are muddy sand and sand. Resistive areas surrounding bore TIN1LC correspond to materials of the Bridgewater Formation, whereas similar areas surrounding bore TIN5LC are associated with Loxton-Parilla Sands.

**Table 3.** Average ECa values between 6-8 m of the 5 boreholes.

| <b>Borehole</b> | <b>Lithologic Unit at 6 to 8 m depths</b> | <b>Averaged Down-hole Electrical Conductivity at 6 to 8 m depths mS/m</b> |
|-----------------|---|---|
| TIN1LC          | Bridgewater Fm                            | 75  |
| TIN3HC          | lagoonal facies                           | 350   |
| TIN4HC          | lagoonal facies                           | 400   |
| TIN5LC          | Loxton-Parilla Sands                      | 150   |
| TIN6HC          | lagoonal facies                           | 600   |



**Figures 18a – d.**

Close-up view of the electrical conductivity patterns surrounding the 5 boreholes (CDI at 6-8 m depths). Areas with high conductivity (appears red) depicts the presence of sandy mud and sandy clay whereas areas with low conductivity (as blue) suggests the presence of sand, or carbonate sand (TIN1LC).

### 6.3 Validation of Constrained Inversion Product – Clay Thickness Image

The Clay Thickness Image, as shown in Figure 7, was derived from the constrained inversion of the RESOLVE data, using a three layer model. The image shows the thickness conductors which are associated with fine-textured materials, *i.e.* sandy mud and sandy clay comprising phyllosilicate minerals.

To enhance the visualisation of the spatial distribution and thicknesses of the fine textured sediments, four pseudo-coloured images were produced by adjusting the maximum thickness value using a look-up-table (LUT) histogram (linear stretch). The reds in Figures 19a – d show areas where the predicted clay thickness is greater than 5 m, 10 m, 15 m and 20 m respectively.

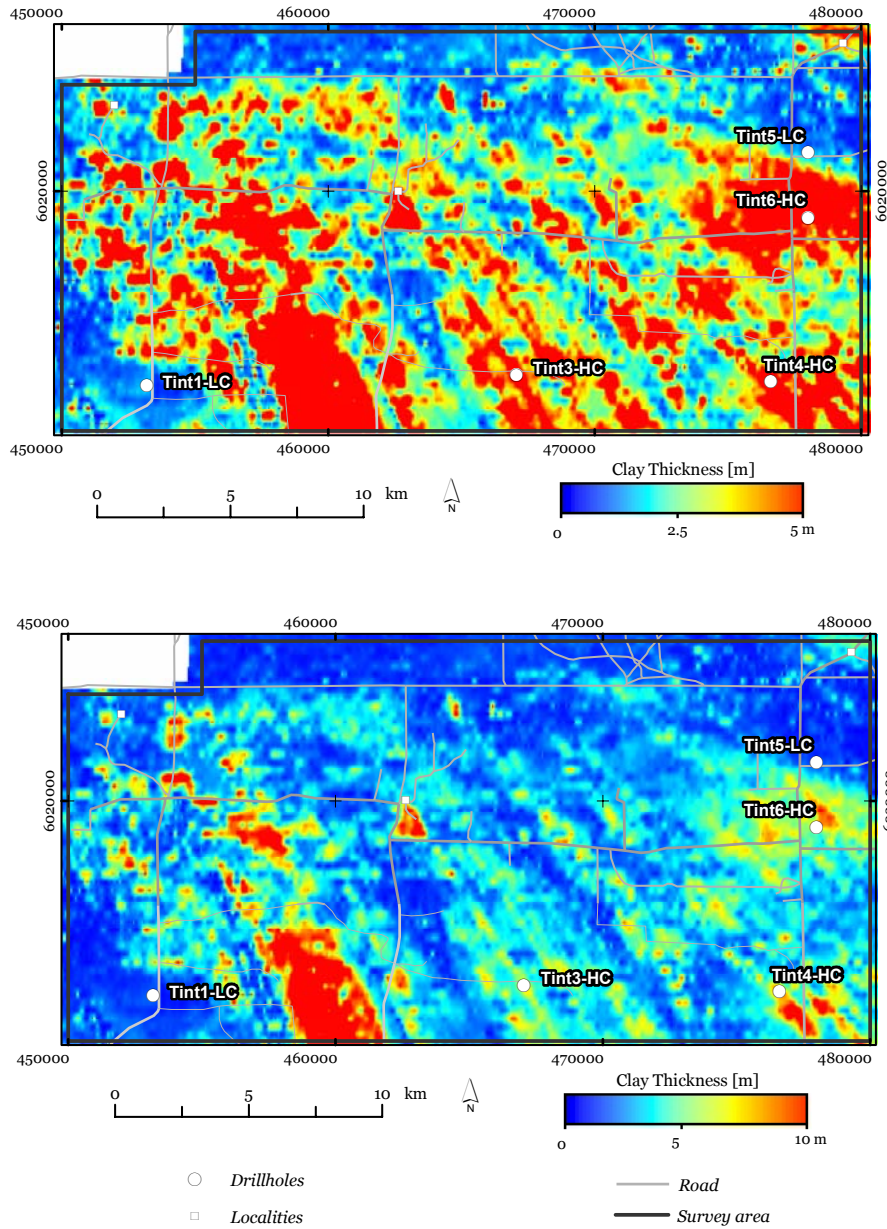
The Clay Thickness Image (Figure 19a) shows that the fine textured sediments are widespread across the study area, with the thicknesses mostly greater than 5 m, but generally less than 10 m (Figure 19b). This is in accord with the borehole information (Table 5), which indicates that the conductive sandy mud and sandy clay of the lagoonal facies are approximately 8 to 11 m thick (Table 5). An exception is the presence of a spatially expansive clay unit which reaches, in part, more than 20 m thick (Figures 19c and 19d). Unfortunately, this could not be verified as no record or borehole information is available. Nevertheless, the limited available borehole information shows that the spatial extent and the thickness of the conductor derived from the geophysical data can be considered as a good surrogate for the thickness of mud and clay.

**Table 4.** Thickness of conductive sediments of the Pliocene lagoonal Facies.

| <b>Borehole</b> | <b>Thickness of Mud and Clay (m)</b> | <b>Predicted Thickness of Conductive Mud (m)</b> |
|-----------------|--------------------------------------|--|
| TIN1LC          | 0                                    | 2  |
| TIN3HC          | 8                                    | 7  |
| TIN4HC          | 11                                   | 9  |
| TIN5LC          | 2                                    | 1  |
| TIN6HC          | 8                                    | 8  |

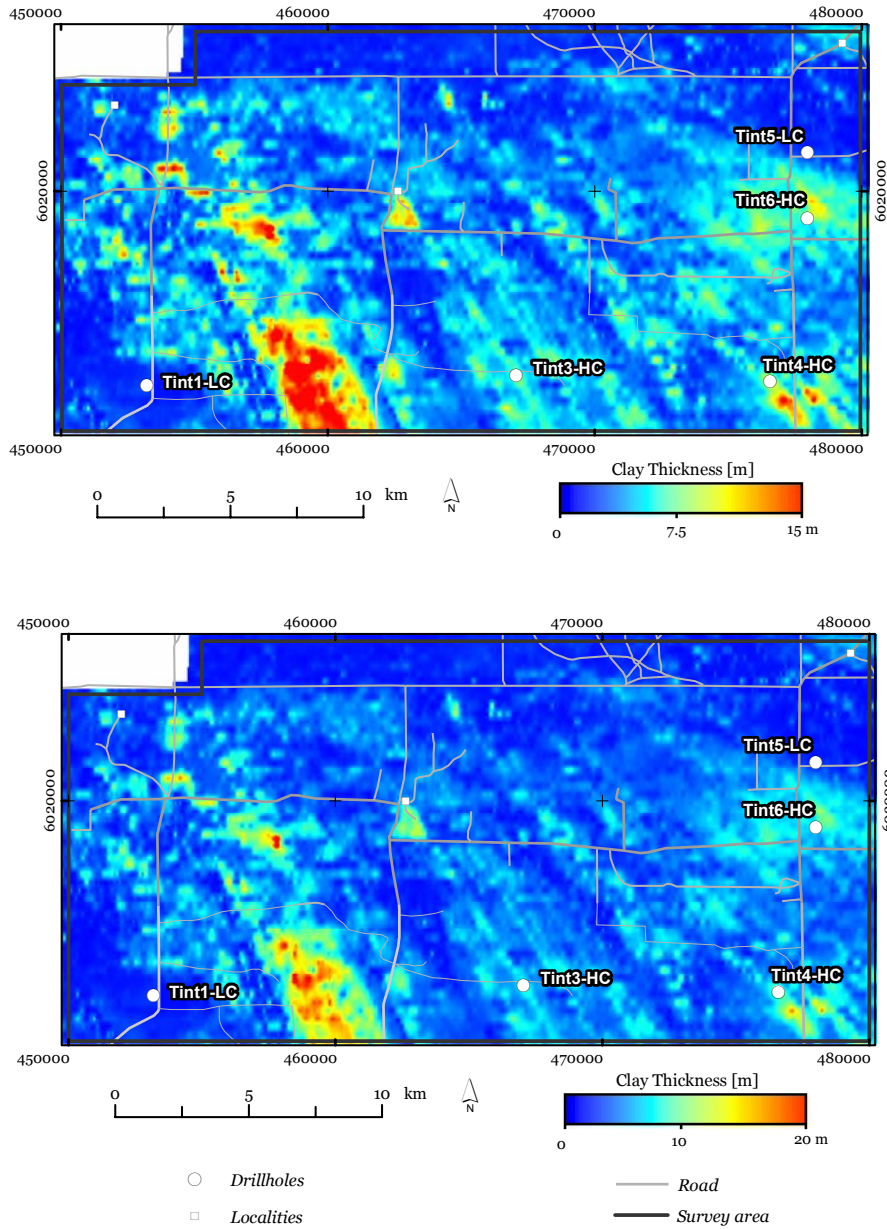
Understanding the sedimentary system also facilitates the interpretation of the airborne EM data. The Pliocene barrier sand and the back barrier lagoonal facies sediments form linear pairs of resistors and conductors respectively. This barrier system forms a time series as the barriers prograded in a westerly direction. A transgressive marine event occurred during the Quaternary caused the partial erosion of this barrier system and the deposition of Bridgewater Formation (younger barrier sand / carbonate sand). Underlying these barrier system sediments are the preserved Loxton-Parilla Sands, comprising shore and shallow marine facies. The schematic block diagram (Figure 20) illustrates the sedimentary relationships and the distribution of fine-textured back barrier sediments as indicated by the geophysical data.

Figures 19a and 19b



**Figures 19a – b.** Constrained inversion product, Conductance Thickness Image (CTI) showing, in red, the thicknesses of conductive clay-rich materials (*i.e.* clay > 5 m and clay > 10 m thick for Figures 19a & 19b respectively).

Figures 19c and 19d



**Figures 19c – d.** Constrained inversion product, Conductance Thickness Image (CTI) showing, in red, the thicknesses of conductive clay-rich materials (*i.e.* clay > 15 m and clay > 20 m for Figs 19c & d respectively).

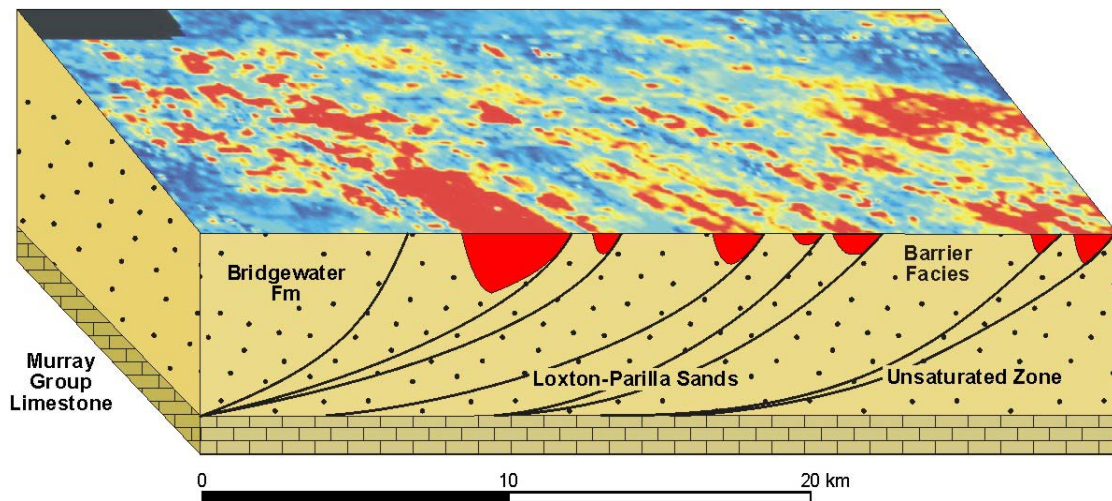


**Figure 20.** Schematic diagram (vertically exaggerated) showing the sedimentary relationships and the distribution of fine-textured back barrier sediments (in red). The thickness of the conductive lagoonal facies sediments have been drawn according to that shown on the Clay Thickness Image (Figures 19a-d).

In the northern part of the HEM inversion products (Figure 21), a resistive area is defined ( $< 150$  mS/m) with a relatively straight southern edge. This boundary coincides with the presence of the Ngarkat Conservation Park, which has abundant native vegetation. Considering the northwesterly alignment of the resistive barrier sand and conductive back barrier sediments, it is reasonable to expect some moderate conductors (yellow-green patches associated with sandy clay) extending beyond the survey area through the northern boundary. Thus, the conspicuous resistor occupied by the native vegetation may be attributed to the efficient abstraction of pore water from the sediments by the plants, resulting in low water content (*i.e.* decreasing degree of pore saturation) and low salt load. Although no bore hole information is available, the predicted textures within the Ngarkat Conservation Park are dominantly sand and muddy sand (Figure 21, blue and greenish blue areas), with minor conductive sandy mud (Figure 21, green and yellow green). The predicted thickness of the sandy mud is approximately 2 m (Figure 19a).

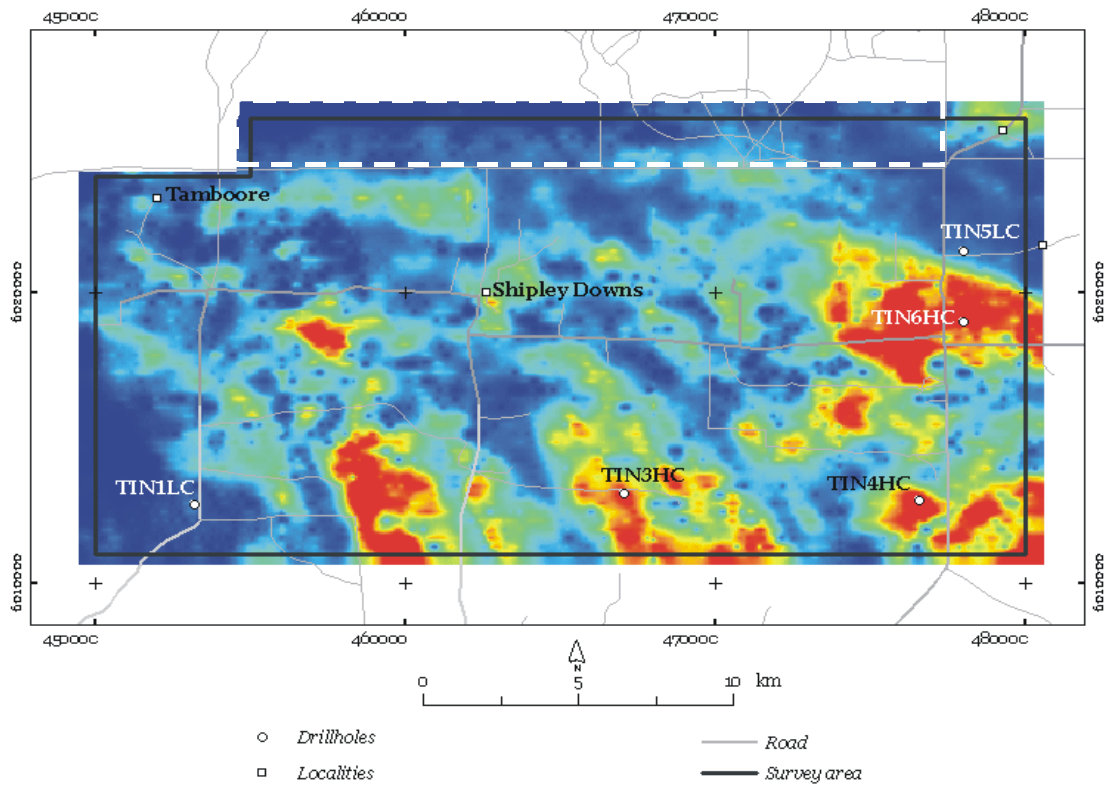


**Figure 21.** RESOLVE<sup>®</sup> HEM interval conductivity for 8-10 m below the surface, derived from a CDI transformation of those data. The Ngarkat conservation park occupies the area bounded by the dotted line.

## 7. CONCLUSIONS

1. In the Tintinara AEM survey area, the primary driving factor of electrical conductivity is salt load, which is a function (product) of water content and its salinity. Electrical conductivity is correlated to clay abundance which, in turn, has a positive causal relationship with water content.
2. The 25<sup>th</sup> percentile of 240 mS/m of the fine-textured lagoonal facies sediments can be used as a threshold value in differentiating between conductive and resistive sediments. From line of regression, 240 mS/m equates to approximately 24 vol. % clay. The sedimentary texture ternary diagram indicates that samples containing more than 24 vol. % clay comprise sandy mud and sandy clay. Since the sands (*i.e.* muddy sand and sand) are dominantly resistive with only a handful of wet and conductive saline sand, it is reasonable to suggest that mud and clay can be mapped using electromagnetic techniques.
3. The petrophysical (particularly electrical) characteristics of the principal geological units suggest that a layered model could be used in the constrained inversion of the HEM data. The layers would comprise an upper resistive layer 1 (Molineaux-Lowan Sands), a conductive layer 2 (lagoonal facies) and a lower resistive layer 3 (Loxton-Parilla Sands).
4. Evidence from textural information and borehole conductivity logs, as obtained from the 5 selected boreholes which targeted specific conductivity signatures shown in the HEM data confirms the validity of using CDI and inversion products for mapping clay distribution. The conductivity patterns suggest the presence of paired linear resistors comprising barrier sand, which is accompanied by conductive back barrier fine-textured sediments.

## 8. REFERENCES

- Barnett, S.R. 2002. Water Resource Assessment of the Tintinara-Coolnalpyn Prescribed Wells Area. Department of Water, Land and Biodiversity Conservation. Report DWLBC 2002/20. 53 pp.
- Brady, N.C. 1990. The Nature and Properties of Soils. McMillan Publishing Company, New York: 621 pp.
- Brown, C.M. and Stephenson, A.E. 1991. Geology of the Murray Basin, Southeastern Australia. BMR Bulletin 235. 430 pp.
- Cowey, D., Garrie, D. and Tovey, A. 2003. Riverland and Tintinara, South Australia, RESOLVE Geophysical Survey, acquisition and processing report. Report to the Bureau of Rural Sciences, available from Geoscience Australia.
- Fraser, D.C., 1978, Resistivity mapping with airborne multicoil electromagnetic system. Geophysics, V43, 144-172.
- Gardner, G.J., Mortlock, A.J., Price, D.M., Readhead, M.L. and Wasson, R.J. 1987. Thermoluminescence and Radiocarbon dating of Australian Desert Dunes. Australian Journal of Earth Sciences, 34, 343-357 pp.
- George, R. and Green, A.A., 2000. Position paper on airborne geophysics for salinity and land management. Sustainable Land and Water Resources Management Committee (SLWRMC) ([ftp://ftp.ndsp.gov.au/pub/general/10\\_NDSP\\_projects/15\\_project\\_reports/RG\\_R\\_VH\\_SLWRMC.pdf](ftp://ftp.ndsp.gov.au/pub/general/10_NDSP_projects/15_project_reports/RG_R_VH_SLWRMC.pdf))
- Green, A.A., Brodie, R.C., and Munday, T.J., 2003, Constrained Inversion of RESOLVE Airborne Electromagnetic Data, Riverland, South Australia, CRCLEME Technical Report 152, 36pp.
- Jones, G. and Henschke, C. 2003. South Australia Salinity Mapping and Management Support: Jamestown drilling Report. A draft report to the technical committee.
- Leaney, F., Walker, G., knight, J., Dawes, W., Bradford, A., Barnett, S. and Stadter, F. 1999. Potential for groundwater salinisation in the Tintinara area of South Australia. Impacts of planned irrigation allocations. CSIRO Land and Water Technical Report 33/99. 57 pp.
- Leaney, F. 2000. Groundwater salinisation in the Tintinara area of South Australia. Results of field investigations. CSIRO Land and Water Technical Report 34/00. 44 pp.
- Lewis, D.W. and McConchie, D. 1994. Practical Sedimentology. Chapman and Hall, New York. 213 pp.
- Macnae, J.C., King, A., Stolz, N., Osmakoff, A. and Blaha, A., 1998, Fast AEM data processing and inversion. Exploration Geophysics, 29, 163-169.

- Moore, D.M. and Reynolds, Jr. R.C. 1989. X-ray Diffraction and the Identification of Clay Minerals. Oxford University Press, Oxford.
- Munday, T.J., Green, A.A., Brodie, R.C., Lane, R., Sattel, D., Barnett, S.R., Cook, P.G. and Walker, G. 2003 Developing recharge reduction strategies in the Riverland of South Australia using airborne electromagnetic data – a case study in tailoring airborne geophysics given a particular target and a desired set of outcomes. Extended abstracts, 16<sup>th</sup> ASEG 2003 Conference, Adelaide. 4pp.
- Rawle, A. 2001. Basic Principles of Particle Size Analysis. Technical Paper MRK043. Malvern Instruments Limited. 8 pp.
- Rhoades, J.D., Raats, P.A.C. and Prather, R.S. 1976. Effects of Liquid-Phase Electrical Conductivity, Water Content and Surface Conductivity on Bulk Soil Electrical Conductivity. In Soil Science Society of American Journal. 40, 651-665 pp.

## **9. ACKNOWLEDGEMENTS**

The Tintinara-East AEM survey was funded by the South Australia Salinity Mapping and Management Support Project (SA-SMMSP), under the auspices of the National Action Plan. Steve Barnett (DLWBC) is thanked for providing groundwater and salinity information and additional borehole data. Megan LeFournour (CSIRO L&W) is thanked for laboratory analysis of drill cores and cuttings. The authors expressed gratitude to John Spring (BRS) for acquiring the down-hole geophysical logs. Heike Apps and Penny Kilgour (GA) have assisted in the GIS and are much appreciated. Thanks also to the land holders and companies for allowing access to drill sites. David Gibson (GA), Ross Brodie (GA/ANU), Andrew FitzPatrick (GA), Mathew Gray (GA), Ken Lawrie (GA), Jonathan Clarke (GA), and Andy Green (OTBC) are thanked for pertinent discussion on geomorphology, groundwater, geology and geophysics. Mary Walsh (GA) is thanked for her administrative assistance.

## **10. APPENDICES**

### **10.1. APPENDIX 1 – METHODS**

#### ***10.1.1 Borehole***

Borehole TIN4HC was drilled using hollow stem auger coring which allow half metre continuous cores to be collected. The core was split into halves, with half the core stored in glass jars and sent for soil-water content and soil-water Cl analyses. The other half was stored in core-trays for lithology logging, grain size and mineralogical analyses. The other 4 boreholes were carried out using rotary air-last (RAB) drilling technique without water injection, and the drill cuttings were collected every metre. The locations and depths of the drill holes are summarised in Table 2. Prior to filling back the holes with drill spoil, the downhole electrical conductivity and gamma responses were measured.

#### ***10.1.2 Down-hole Electrical Conductivity Log***

The down-hole conductivity logs were measured using an inductive conductivity probe (the Auslog-Scintrex A34). Conductivity is measured in milliSiemens per metre (mS/m) and the instrument was calibrated using calibration rings of 100, 300 and 1000 mS/m prior to logging. A polynomial function was utilised by the software AUSWIN to transform the calibrated values. Two sets of logs were recorded as the probe was lowered, then retrieved, at a speed of 5 m per minute and values were recorded every 0.05 m (5 cm) interval. The best set of log (with no/least anomalous artefacts) was then utilised for interpretation (Jones and Henschke, 2003).

#### ***10.1.3 Down-hole Gamma Log***

The down-hole conductivity logs were measured using Auslog-Scintrex A75 gamma tool. The natural gamma radiation was recorded in three-bands (ie. K, U, Th) as counts per seconds and subsequently converted to the standard units API (American Petroleum Institute) using the software AUSWIN. Same as the down-hole conductivity logs, two sets of logs were recorded as the probe was lowered, then retrieved, at a speed of 5 m per minute and values were recorded every 0.05 m (5 cm) interval. The best set of log (with no/least anomalous artefacts) was then utilised for interpretation (Jones and Henschke, 2003).

#### ***10.1.4 Grain Size Distribution***

48 samples, each weighing approximately 20 g, were analysed for particle size using the Mastersizer™ laser diffraction instrument produced by Malvern Instruments. The laser diffraction instrument consists of three parts, a laser source (He-Ne gas or diodes emitter), detectors, and sample chamber that allows suspended particles to recirculate in front of the laser beam (Figure 22).

The Mie theory was used to solve the equations for interaction of light with matter and calculates the volume of the particle. This technique calculates the % volume of a range of particle sizes

(0.05 – 2000  $\mu\text{m}$ ), and the results (Table 6) are grouped according to the Wentworth scale. To standardise with other analytical data, SI units ( $\mu\text{m}$ ) were reported instead of Phi units (Table 5).

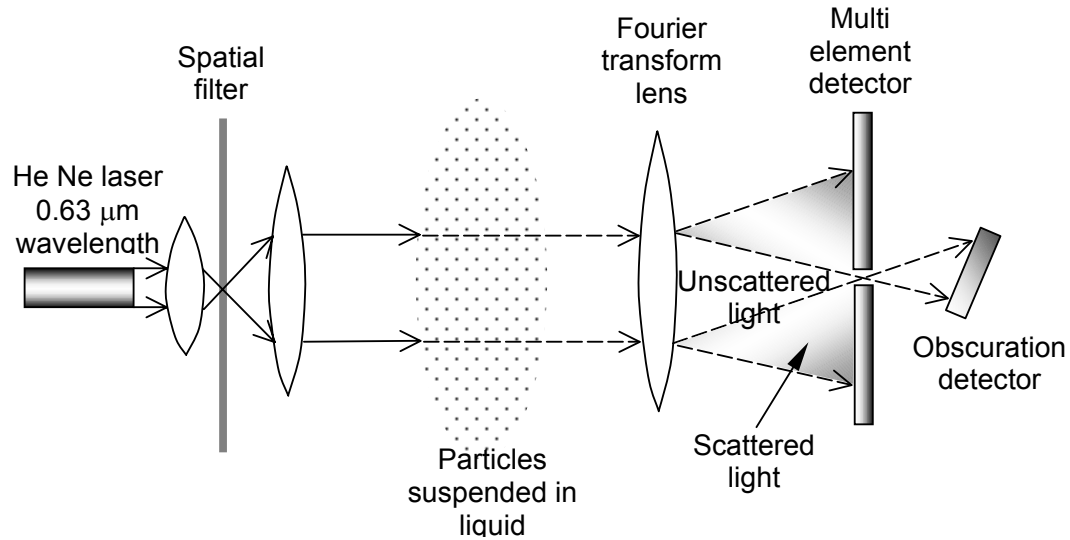


**Figure 22.** Schematic diagram shows the main components of a laser diffractometer. This technique allows the calculation of size fractions in volume % rather than weight %, such as those calculated using the sieving method. Source: From Rawle (2001).

**Table 5.** Particle size in SI units ( $\mu\text{m}$ ), Wentworth scale.

| Size Fraction    | Lower boundary | Upper boundary |
|------------------|----------------|----------------|
| Very coarse sand | 1000           | 2000           |
| Coarse sand      | 500            | 1000           |
| Medium sand      | 250            | 500            |
| Fine sand        | 125            | 250            |
| Very fine sand   | 62.5           | 125            |
| Coarse silt      | 31             | 62.5           |
| Medium silt      | 15.6           | 31             |
| Fine silt        | 7.8            | 15.6           |
| Very fine silt   | 4              | 7.8            |
| Clay             | 0.06           | 4              |

### ***10.1.5 Mineral Composition***

19 samples taken from the 5 boreholes (TIN1LC, TIN3HC, TIN4HC, TIN5LC and TIN6HC) were analysed for mineral composition, using the x-ray diffraction (XRD) technique. Results are shown in Table 7.

Individual samples were homogenised before approximately 5 g was removed and ground in a mortar and pestle, with the addition of ethanol, to a fine, talc-like consistency (1-10  $\mu\text{m}$ ), so as to optimise diffraction (Moore and Reynolds, 1989). Each finely crushed sample was dried and randomly packed into a U-shaped aluminium holder covered with frosted glass slide (to overcome preferred orientation of crystallites). The glass slide was then removed and most samples were analysed using a Siemens™ D5000 series X-ray diffractometer (Co-K $\alpha$ ), and scanned from 4° to 80° 2 $\theta$ , at a speed of 2° per minute, and a step size of 0.02°. The remainder were analysed using a Siemens™ D501 (Cu-K $\alpha$ ), and scanned from 2° to 70° 2 $\theta$ , at a speed of 2° per minute, and a step size of 0.02°. The results were displayed as graphs with the x-axis denoting the 2 $\theta$ ° and the y-axis the diffraction intensity. The mineral identification software EVA™ was used to identify the d-spacings of a series of peaks corresponding to individual minerals.

## 10.2. APPENDIX 2 – ANALYTICAL RESULTS

**Table 6.** Grain size distribution (in  $\mu\text{m}$ ) of sediments and the respective lithologic units.

|          |         | Clay | Silt     | Fine Sand  | Med Sand  | Coarse & VC. Sand | Interpreted                  |
|----------|---------|------|----------|------------|-----------|-------------------|------------------------------|
| Borehole | Depth m | <4   | 4 - 62.5 | 62.5 - 250 | 250 - 500 | 500 - 2000        | Unit                         |
| TIN1LC   | 0.5     | 1.7  | 2.6      | 60.4       | 34.2      | 1.2               | <i>Molineaux-Lowan Sands</i> |
| TIN1LC   | 1.5     | 1.9  | 2.5      | 66.8       | 28.4      | 0.4               | <i>Molineaux-Lowan Sands</i> |
| TIN1LC   | 2.5     | 7.4  | 8.5      | 51.0       | 28.7      | 4.4               | <i>Bridgewater Fm</i>        |
| TIN1LC   | 4.5     | 4.6  | 4.2      | 61.7       | 27.2      | 2.3               | <i>Bridgewater Fm</i>        |
| TIN1LC   | 6.5     | 17.0 | 24.1     | 39.6       | 18.0      | 1.3               | <i>Bridgewater Fm</i>        |
| TIN1LC   | 8.5     | 33.8 | 14.8     | 36.0       | 13.6      | 1.9               | <i>Bridgewater Fm</i>        |
| TIN1LC   | 10.5    | 16.5 | 12.8     | 53.6       | 15.6      | 1.5               | <i>Bridgewater Fm</i>        |
| TIN1LC   | 12.5    | 14.3 | 13.9     | 54.7       | 16.3      | 0.8               | <i>Bridgewater Fm</i>        |
| TIN1LC   | 14.5    | 35.1 | 16.5     | 30.7       | 13.8      | 3.8               | <i>Bridgewater Fm</i>        |
| TIN1LC   | 16.5    | 32.1 | 13.5     | 40.5       | 13.2      | 0.8               | <i>Bridgewater Fm</i>        |
| TIN3HC   | 0.5     | 11.2 | 6.7      | 46.5       | 27.9      | 7.6               | <i>lagoonal facies</i>       |
| TIN3HC   | 1.25    | 40.0 | 18.1     | 20.0       | 13.1      | 8.8               | <i>lagoonal facies</i>       |
| TIN3HC   | 2.25    | 11.8 | 10.3     | 57.8       | 20.0      | 0.0               | <i>lagoonal facies</i>       |
| TIN3HC   | 4.25    | 49.8 | 20.7     | 19.1       | 8.8       | 1.6               | <i>lagoonal facies</i>       |
| TIN3HC   | 6.25    | 34.6 | 30.9     | 25.4       | 8.9       | 0.2               | <i>lagoonal facies</i>       |
| TIN3HC   | 8.25    | 31.3 | 58.0     | 2.5        | 3.1       | 5.1               | <i>lagoonal facies</i>       |
| TIN3HC   | 10.25   | 41.2 | 29.2     | 15.8       | 10.3      | 3.6               | <i>lagoonal facies</i>       |
| TIN3HC   | 12.5    | 18.9 | 29.3     | 32.0       | 13.0      | 6.7               | <i>lagoonal facies</i>       |
| TIN3HC   | 14.5    | 19.6 | 23.1     | 13.6       | 28.7      | 15.0              | <i>lagoonal facies</i>       |
| TIN3HC   | 16.5    | 1.3  | 0.7      | 67.2       | 30.8      | 0.0               | <i>Loxton-Parilla Sands</i>  |
| TIN3HC   | 18.5    | 4.7  | 4.6      | 70.2       | 20.6      | 0.0               | <i>Loxton-Parilla Sands</i>  |
| TIN3HC   | 21.5    | 1.7  | 0.6      | 66.4       | 31.2      | 0.0               | <i>Loxton-Parilla Sands</i>  |
| TIN4HC   | 0.5     | 12.4 | 8.1      | 51.1       | 27.4      | 1.1               | <i>Molineaux-Lowan Sands</i> |
| TIN4HC   | 1.5     | 18.5 | 11.5     | 42.3       | 25.4      | 2.3               | <i>Molineaux-Lowan Sands</i> |
| TIN4HC   | 2.5     | 23.0 | 26.9     | 38.9       | 11.1      | 0.0               | <i>lagoonal facies</i>       |
| TIN4HC   | 4.5     | 30.5 | 33.7     | 26.7       | 8.5       | 0.6               | <i>lagoonal facies</i>       |
| TIN4HC   | 6.5     | 37.3 | 28.4     | 22.8       | 10.4      | 1.0               | <i>lagoonal facies</i>       |
| TIN4HC   | 8.5     | 22.4 | 24.4     | 31.1       | 18.2      | 3.8               | <i>lagoonal facies</i>       |
| TIN4HC   | 10.5    | 3.5  | 3.7      | 63.4       | 29.4      | 0.0               | <i>lagoonal facies</i>       |
| TIN4HC   | 14.5    | 3.1  | 4.1      | 63.3       | 29.4      | 0.0               | <i>Loxton-Parilla Sands</i>  |
| TIN4HC   | 16.5    | 3.5  | 5.3      | 64.3       | 26.8      | 0.0               | <i>Loxton-Parilla Sands</i>  |
| TIN5LC   | 0.8     | 19.9 | 18.6     | 25.7       | 30.7      | 5.2               | <i>Molineaux-Lowan Sands</i> |
| TIN5LC   | 3.3     | 0.00 | 0.0      | 46.0       | 47.6      | 6.5               | <i>Molineaux-Lowan Sands</i> |
| TIN5LC   | 4.4     | 6.15 | 6.3      | 38.2       | 38.2      | 11.2              | <i>Loxton-Parilla</i>        |

|                           |                |              |                 |                   |                  |                              |                              |
|---------------------------|----------------|--------------|-----------------|-------------------|------------------|------------------------------|------------------------------|
|                           |                |              |                 |                   |                  |                              | Sands                        |
| <b>Table 6. Continued</b> |                |              |                 |                   |                  |                              |                              |
|                           |                | <b>Clay</b>  | <b>Silt</b>     | <b>Fine Sand</b>  | <b>Med Sand</b>  | <b>Coarse &amp; VC. Sand</b> | <b>Interpreted</b>           |
| <b>Borehole</b>           | <b>Depth m</b> | <b>&lt;4</b> | <b>4 - 62.5</b> | <b>62.5 - 250</b> | <b>250 - 500</b> | <b>500 - 2000</b>            | <b>Unit</b>                  |
| TIN5LC                    | 7.4            | 28.3         | 39.3            | 16.9              | 12.9             | 2.6                          | <i>Loxton-Parilla Sands</i>  |
| TIN5LC                    | 8.7            | 15.37        | 40.9            | 32.2              | 10.9             | 0.7                          | <i>Loxton-Parilla Sands</i>  |
| TIN5LC                    | 12.4           | 2.49         | 4.5             | 40.2              | 38.1             | 14.6                         | <i>Loxton-Parilla Sands</i>  |
| TIN5LC                    | 14.7           | 7.4          | 3.6             | 47.3              | 34.0             | 7.7                          | <i>Loxton-Parilla Sands</i>  |
| TIN5LC                    | 18.4           | 1.63         | 3.7             | 62.9              | 30.9             | 0.8                          | <i>Loxton-Parilla Sands</i>  |
| TIN5LC                    | 22.5           | 1.4          | 3.9             | 44.9              | 44.8             | 5.0                          | <i>Loxton-Parilla Sands</i>  |
| TIN6HC                    | 0.5            | 3.5          | 4.5             | 53.0              | 31.9             | 7.1                          | <i>Molineaux-Lowan Sands</i> |
| TIN6HC                    | 1.5            | 14.2         | 14.9            | 38.7              | 27.6             | 4.5                          | <i>Molineaux-Lowan Sands</i> |
| TIN6HC                    | 2.5            | 9.6          | 7.6             | 51.9              | 29.9             | 0.9                          | <i>Molineaux-Lowan Sands</i> |
| TIN6HC                    | 4.5            | 35.0         | 28.2            | 18.3              | 17.2             | 1.3                          | <i>lagoonal facies</i>       |
| TIN6HC                    | 8.25           | 37.0         | 23.8            | 26.8              | 12.1             | 0.3                          | <i>lagoonal facies</i>       |
| TIN6HC                    | 10.25          | 57.3         | 29.0            | 9.7               | 3.9              | 0.0                          | <i>lagoonal facies</i>       |
| TIN6HC                    | 12.25          | 4.2          | 4.9             | 42.6              | 37.3             | 10.9                         | <i>Loxton-Parilla Sands</i>  |
| TIN6HC                    | 13.75          | 3.7          | 4.5             | 39.7              | 36.1             | 16.1                         | <i>Loxton-Parilla Sands</i>  |

**Table 7.** Mineral Composition of sediments and the respective lithologic units.

| Borehole | Depth<br>m | Depth<br>To | Minerals |                 |                 | Interpreted Unit             |
|----------|------------|-------------|----------|-----------------|-----------------|------------------------------|
|          |            |             | Dominant | Less Abundant   |                 |                              |
| TIN1LC   | 4          | 5           | Quartz   |                 | Kaolinite       | <i>Bridgewater Fm</i>        |
| TIN1LC   | 8          | 9           | Quartz   | Calcite         |                 | <i>Bridgewater Fm</i>        |
| TIN1LC   | 16         | 17          | Calcite  | Quartz          |                 | <i>Bridgewater Fm</i>        |
| TIN3HC   | 2.5        | 3           | Quartz   |                 | Muscovite       | <i>lagoonal facies</i>       |
| TIN3HC   | 6          | 6.5         | Quartz   | Montmorillonite | Kaolinite       | <i>lagoonal facies</i>       |
| TIN3HC   | 8          | 8.5         | Calcite  |                 | Quartz          | <i>lagoonal facies</i>       |
| TIN3HC   | 12         | 13          | Quartz   | Calcite         | Montmorillonite | <i>lagoonal facies</i>       |
| TIN4HC   | 1          | 2           | Quartz   |                 | Kaolinite       | <i>Molineaux-Lowan Sands</i> |
| TIN4HC   | 6          | 7           | Quartz   | Kaolinite       |                 | <i>lagoonal facies</i>       |
| TIN4HC   | 12         | 13          | Calcite  | Quartz          |                 | <i>lagoonal facies</i>       |
| TIN4HC   | 16         | 17          | Quartz   |                 | K-feldspar      | <i>Loxton-Parilla Sands</i>  |
| TIN5LC   | 0.8        | 0.9         | Quartz   |                 | Kaolinite       | <i>Molineaux-Lowan Sands</i> |
| TIN5LC   | 7.4        | 7.5         | Quartz   | Illite          | Kaolinite       | <i>Loxton-Parilla Sands</i>  |
| TIN5LC   | 14.7       | 14.8        | Quartz   |                 | Kaolinite       | <i>Loxton-Parilla Sands</i>  |
| TIN5LC   | 22.5       | 22.6        | Quartz   |                 | Muscovite       | <i>Loxton-Parilla Sands</i>  |
| TIN6HC   | 1          | 2           | Quartz   |                 | Kaolinite       | <i>Molineaux-Lowan Sands</i> |
| TIN6HC   | 4          | 5           | Quartz   | Calcite         | Kaolinite       | <i>lagoonal facies</i>       |
| TIN6HC   | 10         | 10.5        | Quartz   | Kaolinite       |                 | <i>lagoonal facies</i>       |
| TIN6HC   | 13.5       | 14          | Quartz   |                 | Kaolinite       | <i>Loxton-Parilla Sands</i>  |